Article

Cell Systems

Environmental modulators of algae-bacteria interactions at scale

Graphical abstract

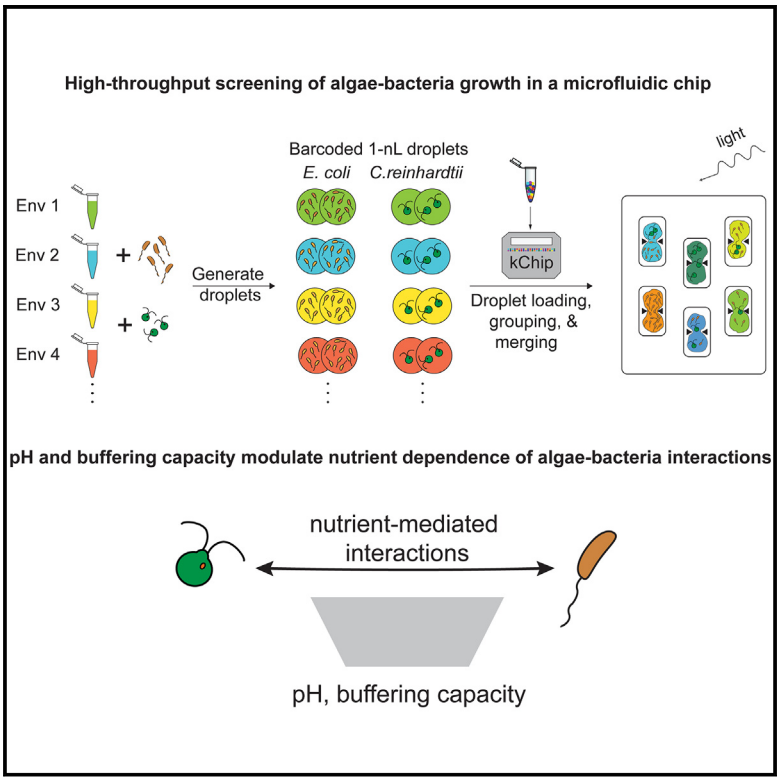

Authors

Chandana Gopalakrishnappa, Zeqian Li, Seppe Kuehn

Correspondence

seppe.kuehn@gmail.com

In brief

Interactions between photosynthetic and heterotrophic microbes occur in chemically diverse environments and are vital to global carbon cycles. Our high-throughput screening of >100,000 algae-bacteria communities in ~525 environments reveals that pH, buffering capacity, and carbon source identity modulate algae-bacteria interactions by impacting the dependence of growth on nutrient availability.

Highlights

- Phototrophic and heterotrophic microbes reside in chemically complex environments
- A microfluidic chip enables measurements on >100,000 phototroph-heterotroph cultures
- Screen algae-bacteria interactions in ~525 environments in monoculture and coculture
- pH, buffering capacity, and carbon source identity modulate algae-bacteria interactions

Gopalakrishnappa et al., 2024, Cell Systems *15*, 1–16
September 18, 2024
https://doi.org/10.1016/j.cels.2024.08.002

CellPress

Cell Systems

CellPress

Article

Environmental modulators of algae-bacteria interactions at scale

Chandana Gopalakrishnappa,[1] Zeqian Li,[1,2,3] and Seppe Kuehn[2,3,4,5,6,*]
[1]Department of Physics, The University of Illinois at Urbana-Champaign, Urbana, IL 61801, USA
[2]Center for the Physics of Evolving Systems, The University of Chicago, Chicago, IL 60637, USA
[3]Department of Ecology and Evolution, The University of Chicago, Chicago, IL 60637, USA
[4]National Institute for Theory and Mathematics in Biology, Northwestern University and The University of Chicago, Chicago, IL 60637, USA
[5]Center for Living Systems, The University of Chicago, Chicago, IL 60637, USA
[6]Lead contact
*Correspondence: seppe.kuehn@gmail.com
https://doi.org/10.1016/j.cels.2024.08.002

SUMMARY

Interactions between photosynthetic and heterotrophic microbes play a key role in global primary production. Understanding phototroph-heterotroph interactions remains challenging because these microbes reside in chemically complex environments. Here, we leverage a massively parallel droplet microfluidic platform that enables us to interrogate interactions between photosynthetic algae and heterotrophic bacteria in >100,000 communities across ~525 environmental conditions with varying pH, carbon availability, and phosphorus availability. By developing a statistical framework to dissect interactions in this complex dataset, we reveal that the dependence of algae-bacteria interactions on nutrient availability is strongly modulated by pH and buffering capacity. Furthermore, we show that the chemical identity of the available organic carbon source controls how pH, buffering capacity, and nutrient availability modulate algae-bacteria interactions. Our study reveals the previously underappreciated role of pH in modulating phototroph-heterotroph interactions and provides a framework for thinking about interactions between phototrophs and heterotrophs in more natural contexts.

INTRODUCTION

Microbial communities occupy nearly every niche on Earth, from animal hosts to soils and oceans. These complex consortia often contain many interactions between members whereby one species impacts the abundance of another. Interactions in these communities can determine the outcome of invasions,[1] metabolic processes, such as carbon and nitrogen remineralization,[2] or the phenotype of the host.[3] Crucially, however, interactions between members of a microbial consortium depend on the environmental context. For example, changes in pH, nutrient availability, temperature, or toxic metabolic byproducts can strongly modulate interactions between members of a collective.[4–8] As a result, an important question in ecology is understanding how environmental parameters impact these interactions.

Understanding how environmental parameters influence ecological interactions between pairs of taxa in communities is challenging. The physicochemical environment in natural microbial communities is high dimensional in the sense that there are many possible parameters that change in time and space and can impact the outcome of an interaction.[9] This high dimensionality means that experimentally interrogating how interactions depend on the environment is a daunting task. For example, to measure the growth of a single strain across all possible combinations of four different environmental variables at 10 levels for each variable (for example, pH, carbon, nitrogen, and phosphorus availability) would require 10^4 experiments. To determine interactions between just two taxa would require measuring their growth alone and in coculture in each one of these conditions—meaning that 30,000 measurements would be required, a huge undertaking.

Here, we address this problem using a massively parallelized droplet microfluidic platform[10] to interrogate interactions between a photosynthetic alga (phototroph) and a heterotrophic bacterium. Phototrophs form the basis of primary production in many environments, and heterotrophic bacteria play an important role in the growth of phototrophic populations both in natural ecosystems and engineered bioreactors.[11,12] One of the key features of phototroph-heterotroph interactions is that they occur between distinct metabolic strategies. Phototrophs are capable of fixing inorganic carbon using light, whereas heterotrophic organisms require chemical energy, often in the form of reduced carbon, to generate energy and biomass. Phototrophs excrete some fraction of the carbon they fix, and this provides the chemical substrates upon which heterotrophic microbes depend. As a result, prior work on phototroph-heterotroph interactions has often focused on the exchange of organic carbon between these two metabolic strategies.[11,13]

Please cite this article in press as: Gopalakrishnappa et al., Environmental modulators of algae-bacteria interactions at scale, Cell Systems (2024), https://doi.org/10.1016/j.cels.2024.08.002

Although the exchange of organic carbon between phototrophs and heterotrophs is important, other environmental factors also play a role and are less well studied. For example, in some nutrient-rich environments, such as estuaries or coastal ecosystems, organic carbon is available to heterotrophs through the decay of organic matter rather than the direct excretion of carbon from phototrophs.[14] In addition, interactions between phototrophs and heterotrophs depend on a host of other environmental factors. For example, the dynamics of phototrophs in association with heterotrophs can depend on the availability of exogenously supplied carbon, nitrogen, and phosphorus, or on temperature, light, pH, and small molecule exchanges.[15–23] Therefore, it appears critical to understand how environmental factors affect interactions in these communities, even when carbon exchange is not the central factor. Most, but not all,[16] previous studies in laboratory model systems have focused on carbon exchange,[11,24–27] leaving a gap in knowledge. Addressing this gap comes with the challenges posed above of measuring interactions at a large enough scale to assess the role of multiple environmental factors. Thus, although carbon exchange between phototrophs and heterotrophs is important, there are also contexts where carbon for bacterial growth is supplied exogenously. In addition, nutrients and environmental variables beyond carbon can play a defining role in the outcome of phototroph-heterotroph interactions, but the role of these variables is less well studied.

To address this problem, we interrogated phototroph-heterotroph interactions in a context where carbon exchange does not play a dominant role in the growth and proliferation of the community, but the role of other environmental factors can be readily assayed at a massive scale. To accomplish this, we used a microfluidic platform that leverages nanoliter droplets, with contents barcoded using fluorescent dyes, to measure abundance dynamics in >20,000 cultures in a single experiment. Using this approach, we measured the interaction between the model alga *Chlamydomonas reinhardtii* (*C. reinhardtii*) and the bacterium *Escherichia coli* (*E. coli*) in ~525 environmental conditions in >10 replicates each for both monoculture and coculture. Using this platform, we quantified the dynamics of algal and bacterial growth over a period of 4 days. On this timescale, the excretion of organic carbon by the alga was small[28]; therefore, we provided exogenous organic carbon to permit bacterial growth to occur.

Within the nanoliter droplets, we measured algae-bacteria abundance dynamics via microscopy across a range of organic carbon sources and concentrations, phosphorus concentrations, pH, and buffering capacities. The resulting dataset proved amenable to statistical analysis, where regression revealed the key environmental drivers of algae-bacteria interactions. Although previous studies suggest that nutrient availability is the key driver of interactions between phototrophs and heterotrophs, we find that pH and buffering capacity qualitatively alter how the availability of nutrients impacts the interaction between algae and bacteria. Thus, we show that across a large range of environmental conditions, pH and the ability of the environment to resist changes in pH (buffering capacity) act as important regulators of the interaction between phototrophs and heterotrophs. Finally, the role of the environmental factors—pH, buffering capacity, and nutrient availability—in regulating interactions is modified by the chemical identity of exogenously available organic carbon. These results suggest that the chemical composition of organic carbon and pH interact to qualitatively determine the outcome of algae-bacteria interactions.

RESULTS

The model system and environmental conditions

The microbial community under study comprises the alga, *C. reinhardtii*, commonly found in soils and freshwater,[29] as the phototroph, and the host-associated and soil-dwelling bacterium,[30,31] *E. coli*, as the heterotroph. We note that these microbes are not known to coexist in the wild; therefore, we expect no strong co-evolutionary history between these organisms. Despite this, these two species represent the essential metabolic strategies of phototrophs and heterotrophs. The alga fixes CO_2, and the bacterium utilizes complex carbon sources for energy and biomass. In addition, given that the droplet microfluidic platform is not readily amenable to longer-term growth assays (>5 days), the relatively rapid growth of the alga (doubling time 8–12 h) enables us to use the platform to interrogate the interaction between these two taxa. Therefore, although these two species do not represent an interacting pair of wild microbes, they are representative of the orthogonal metabolic strategies of phototrophs and heterotrophs while being amenable to measurements at scale. Thus, our intention here is to utilize these taxa as representatives of these metabolic strategies while being cognizant that the insights we gain here will need further validation in other ecological contexts. Despite this limitation, these two microbes have been widely used in studies as model phototrophs and heterotrophs due to their thorough biological characterization, ease of cultivation, and accessibility to molecular techniques and quantitative measurements. Previous studies of closed microbial communities, including these two microbes, in addition to a ciliate, have revealed strongly deterministic dynamics on timescales of months and rich spatiotemporal and phenotypic processes.[32,33] Another study demonstrated the presence of higher-order interactions between this alga and bacteria mediated by a ciliate.[1] Thus, the interactions between these two model organisms constitute a tractable test bed for understanding phototroph-heterotroph interactions.

In this study, interactions between the algae, *C. reinhardtii*, and the bacteria, *E. coli* were assayed in modified Taub media (a freshwater mimic media) that varied in five environmental factors—initial pH, buffering capacity, phosphorus concentration, carbon concentration, and carbon source identity. The chosen environmental factors are among those that significantly contribute to chemical variation across natural environments.[34,35] Although resource competition and exchange are identified as key players in driving phototroph-heterotroph interactions,[11,12,16–19,22,36] several studies have reported a strong correlation between the compositions of microbial communities and environmental factors, such as pH and concentration of nutrients—carbon, nitrogen, and phosphorus.[37–39] Additionally, it is well known that the identity of the carbon source affects *E. coli* metabolism via impacting growth rate and the nature of the metabolic products, which could potentially lead to different interactions with *C. reinhardtii*.[40–42] Therefore, we reasoned that a multitude of abiotic factors, such as pH,

Please cite this article in press as: Gopalakrishnappa et al., Environmental modulators of algae-bacteria interactions at scale, Cell Systems (2024), https://doi.org/10.1016/j.cels.2024.08.002

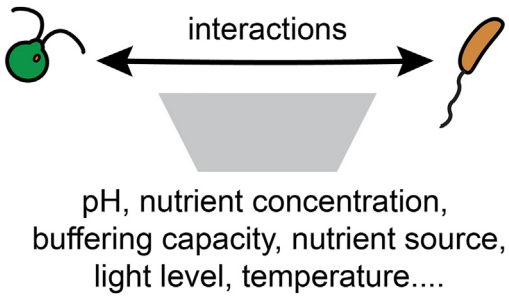

Figure 1. Dependence of algae-bacteria interactions on environmental factors

Illustration of our hypothesis that diverse interactions between algae and bacteria are altered by a multitude of chemical factors in the environments, such as concentration of nutrients, pH, buffering capacity, light level, and temperature.

buffering capacity, light level, including nutrient concentration, and type, may contribute to phototroph-heterotroph interactions (Figure 1). Hence, we chose the above five factors. The values of each of the environmental factors were chosen to be in biologically plausible ranges: 6.1–7.5 for initial pH, ~0–3.5 mM for buffering capacity, 0.01–4 mM for phosphorus concentration, 2–10 mM (carbon atoms) for the carbon concentration (STAR Methods). We chose five different carbon sources (glycerol, glucose, galactose, pyruvate, and acetate) to assay both gluconeogenic and glycolytic carbon sources, as well as a carbon source that is known to support mixotrophic growth of the alga (acetate). For each of these carbon sources, the algae-bacteria interactions were assayed in a total of ~105 environmental conditions for monoculture of each taxon and coculture of both.

High-dimensional characterization of phototroph-heterotroph interactions

In this study, we used droplet-based microfluidic chip ("kChip" with k = 2) to rapidly assay the phototroph-heterotroph interactions in hundreds of environmental conditions in parallel. The kChip platform has previously been utilized for drug discovery, pathogen detection, and the study of bacterial interactions.[10,43–45] Briefly, the experiment proceeds by first generating a library of environmental conditions that vary in the initial pH, buffering capacity, concentration of phosphorus, and concentration of carbon of a chemically defined minimal medium (Figure 2A; STAR Methods). Initial pH refers to the starting pH of the environment, which we varied by using buffers and titration. To vary the buffering capacity of the environment, we added different concentrations of organic buffers (Tris or MOPS) that cannot be used as nutrient sources by algae or bacteria (Figure S21). We fluorescently barcoded each environmental condition using three fluorescent dyes in low concentrations and added algae and bacteria independently. Using these precultures, a commercial droplet generator was used to create thousands of nanoliter water-in-oil droplets containing algae or bacteria in each of the predefined nutrient conditions. These droplets were then pooled and loaded into a kChip microfluidic chip platform, which contains ~25,000 microwells, each of which randomly groups two droplets containing microbes in predefined media conditions, resulting in the formation of all possible combinations of communities (monocultures and cocultures) and environmental conditions (Figure 2A; STAR Methods). The chip is then imaged to identify the fluorescent dye barcodes and thereby infer the environmental conditions present in each microwell (STAR Methods). Subsequently, the droplets in each microwell were merged via exposure to an alternating electric field, leading to the formation of the phototroph-heterotroph communities in hundreds of environmental conditions. Thereafter, the kChip was incubated at 30°C under light (68.5 μmol $m^{-2}s^{-1}$) to allow for growth. The chip was then imaged at regular intervals (approximately 0, 12, 21, 45, and 68 h) to track the growth of the microbes using chlorophyll fluorescence for *C. reinhardtii* and genetically encoded GFP fluorescence for *E. coli* (Figure 2B; STAR Methods). Algal and bacterial abundances over time were determined by analyzing the microscopy images, generating microbial growth curves, and estimating growth as the difference between the initial abundances and the final abundances at the end of the experiment. We performed this analysis for both the phototroph and heterotroph in >100,000 microbial communities constructed in the kChip experiments for all the carbon sources (Figure 2C; STAR Methods and Dataset 1). We quantified total growth, over the 4 days of the experiment rather than growth rates because the low temporal resolution of our measurement seriously limited our ability to quantify growth rates, especially for bacteria which often saturated before the first time point. We note that the abundance of the microbes may not be saturated at the end of the experiment in some of the environmental conditions. This is due to the duration of the experiment being limited by small droplet volumes and evaporation losses. The experiments on the kChip platform were found to be largely reproducible (Figure S20).

Previous studies utilizing this platform studied bacteria. Therefore, we modified existing protocols to make the measurement compatible with algae. Specifically, we added the functionality for imaging chlorophyll fluorescence to track the growth of *C. reinhardtii* and devised a computational pipeline to remove the bleed-through between chlorophyll fluorescence and one of the barcoding dyes (STAR Methods). This expanded the number of fluorophores that can be probed on the kChip from four to five.

Patterns in interactions between algae and bacteria

To begin, we compared the growth of both algae and bacteria in cocultures with their growth in monocultures. To visualize this, we plotted the growth in cocultures against the growth in monocultures. The dashed lines indicate equal growth in coculture and monoculture. Points below the dashed line indicate competitive or inhibitory interactions, and points above the dashed line indicate facilitation. The bacterial growth in cocultures was lower than their respective growth in monocultures in all the environmental conditions, suggesting inhibition of *E. coli* by *C. reinhardtii* (Figures 3A and S8). Additionally, the *E. coli* cells show greater aggregation in monocultures than in cocultures (Figure S6). These results are consistent with a previous study that showed that introducing bacteria into algal cultures results in the inhibition of bacterial growth and the dispersal of bacterial aggregates.[1]

C. reinhardtii, on the other hand, has similar growth in cocultures and monocultures in most cases, indicating a weak effect of *E. coli* on the growth of *C. reinhardtii* (Figures 3B and S9).

Please cite this article in press as: Gopalakrishnappa et al., Environmental modulators of algae-bacteria interactions at scale, Cell Systems (2024), https://doi.org/10.1016/j.cels.2024.08.002

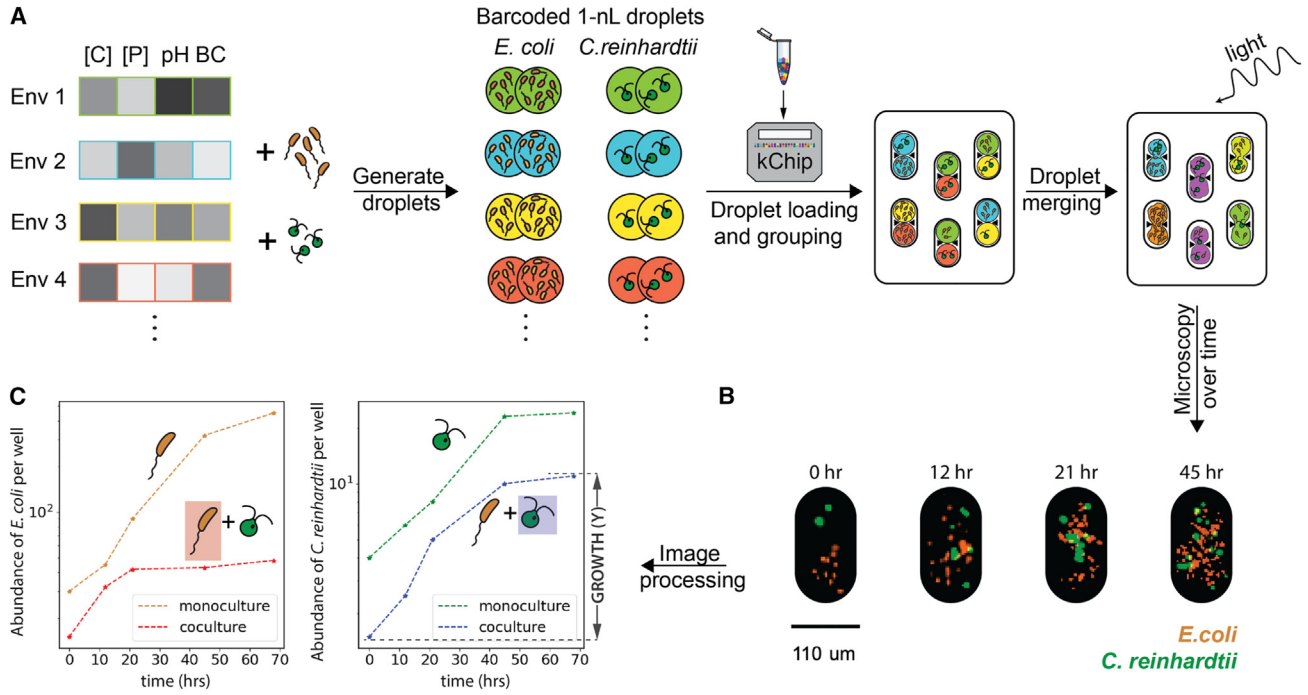

Figure 2. A high-throughput droplet platform for measuring algae-bacteria growth in hundreds of environments

(A) Setting up the microfluidic chip. Environments (media conditions) varying in the factors—initial pH, buffering capacity, phosphorus concentration, and carbon concentration—are prepared and barcoded using three fluorescent dyes (STAR Methods). After adding the bacteria (brown) and algae (green) independently to each barcoded media, nanoliter droplets of each of the microbes in the barcoded environments are generated. The generated droplets are pooled together and loaded on the microfluidic chip, which randomly groups two droplets in each of its microwells. The chip is then imaged for fluorescent barcodes using a widefield fluorescence microscope to infer the values of the environmental factors in the microwells via image processing (STAR Methods). Following exposure of the chip to an alternating electric field, droplets in the microwells merge to form replicates of bacterial monocultures, algal monocultures, and algae-bacteria cocultures in all combinations of the environments that were present in the initial droplets. The chip is then incubated at 30°C under light (68.5 μmol $m^{-2}s^{-1}$).

(B) Microscopy images of a single microwell showing the growth of algae and bacteria over time. The GFP fluorescence image representing the bacteria (in brown) and the chlorophyll fluorescence image representing the algae (in green) are overlayed in these images. The first image shows the bacteria and the algae in the separate compartments of the well, prior to the merging of the droplets. The later images show the increase in the abundance of the algae and bacteria at 12, 21, and 45 h.

(C) Example growth curves of algae and bacteria in monoculture and coculture in an environmental condition. The images of the chip are analyzed to infer the abundances of the microbes in the microwells over time (STAR Methods). The growth *Y* of algae and bacteria are then obtained by estimating the increase in their respective abundances at 68 h from their abundances at 0 h (black arrow labeled "GROWTH (*Y*)" right panel).

There do exist a few environments where *C. reinhardtii* is suppressed or enhanced in coculture relative to monoculture (points lying considerably below or above the dashed line in Figure 3B), indicating an impact of the presence of the bacteria.

Further, we observe that interactions tend to be inhibitory or competitive in conditions where monoculture growth is substantial and facilitative when monoculture yields are low. To see this examine Figure 3B (and Figure S9) where algal growth tends to lie below the dashed line at high values along the x axis and the opposite at low values. This trend is conserved across all environmental conditions. We observe a similar trend for the bacteria. Although *E. coli* is inhibited by algae in all conditions assayed (all points are below the dashed line, Figure 3A), the inhibition is stronger at high values of monoculture growth and weaker at low values of monoculture growth. If higher values of monoculture growth are interpreted as indicative of more permissive environments, this pattern supports the stress-gradient hypothesis (SGH), which posits that interactions should tend to be competitive in permissive environments and facilitative in stressful environments (see discussion).

Finally, despite the overall reproducibility of our kChip experiments (Figure S20), we observe higher variability in *E. coli* growth than in *C. reinhardtii* growth. Detailed analyses at the single-droplet level reveal this variability to be associated with the stochasticity in the initial cell densities in the kChip wells (STAR Methods and Figure S19).

Algae-bacteria interactions show complex dependence on the environmental factors

Next, we sought to understand the dependence of algae-bacteria interactions on environmental factors. To visualize this, we plotted the growth in cocultures against the growth in monocultures, color-coding the data for each of the four environmental variables considered—initial pH, buffering capacity, and concentration of carbon and phosphorus (Figures 3, S8, and S9). These plots show no distinct grouping of the data based on any of the four environmental factors and indicate a complex dependence of algae-bacteria interactions on environmental factors. For example, in the case of *E. coli*, whereas low carbon concentration (the light green points in Figure 3A, bottom right)

Please cite this article in press as: Gopalakrishnappa et al., Environmental modulators of algae-bacteria interactions at scale, Cell Systems (2024), https://doi.org/10.1016/j.cels.2024.08.002

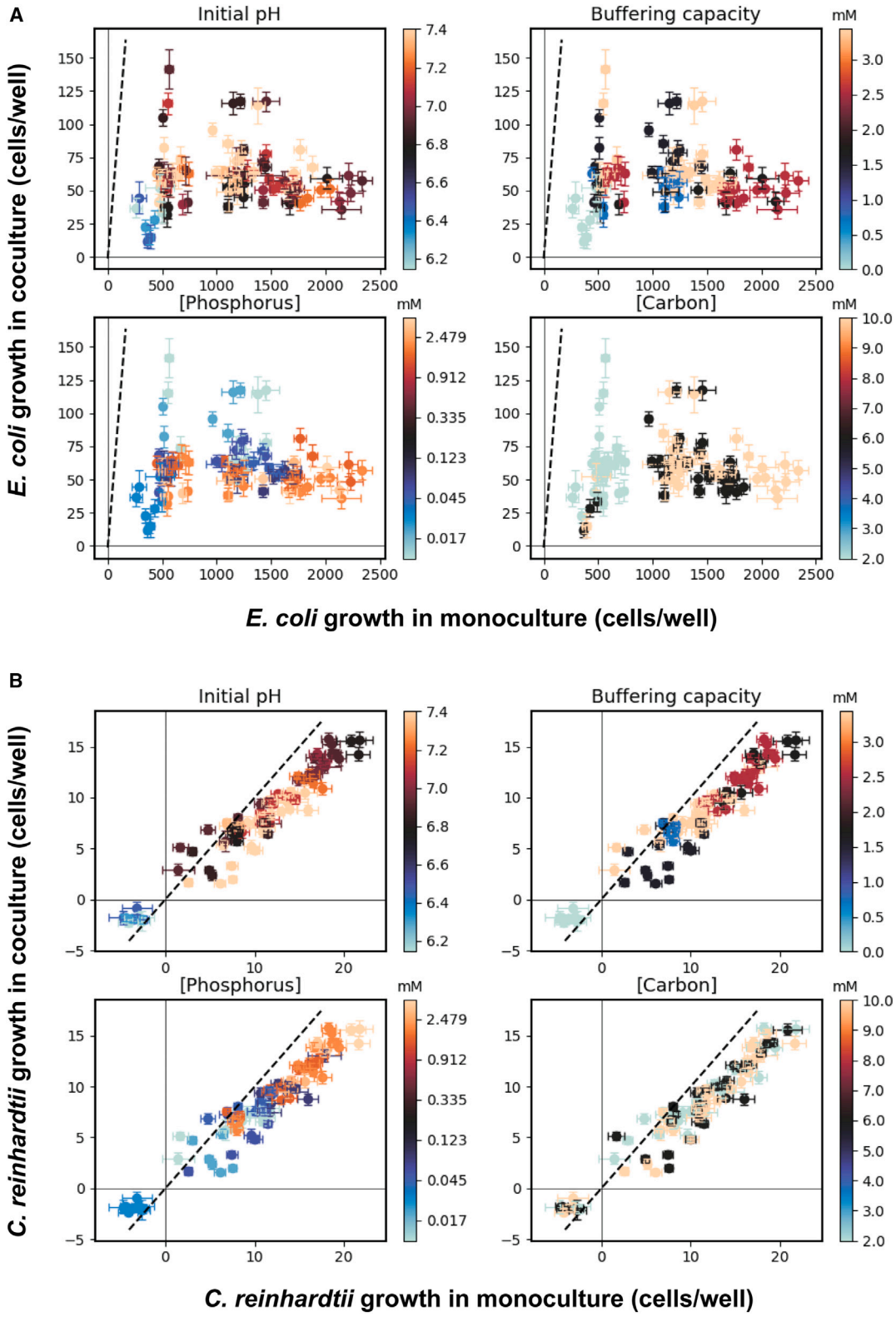

Figure 3. Complex dependence of algae-bacteria interactions on environmental factors

(A) Panels show bacterial growth in monoculture (x axis) and coculture (y axis). Each point indicates median growth (Figure 2C) of *E. coli* in coculture and monoculture computed across replicates of each environmental condition. Error bars indicate the standard error of the mean growth. The median number of replicates per environmental condition ranges from 35–70 for the different culture conditions. The dashed line indicates equal growth in monoculture and

(legend continued on next page)

Please cite this article in press as: Gopalakrishnappa et al., Environmental modulators of algae-bacteria interactions at scale, Cell Systems (2024), https://doi.org/10.1016/j.cels.2024.08.002

sets the growth in monocultures to low values, the variation in other environmental factors (pH, buffering capacity) causes the coculture growth to span from low to high values. There also exist cases where a single environmental factor largely determines monoculture and coculture growth. For example, low buffering capacity, not initial pH, or nutrient availability, appears to give rise to the death of *C. reinhardtii* (light green points have growth less than zero) (Figure 3B, top right).

When we compute correlations between the environmental factors and growth, we see significant statistical relationships between multiple factors and the bacterial or algal growth (Figure S7) across carbon sources. These correlations reinforce the idea that there is a complex interplay between nutrient concentration, pH, buffering capacity, and the identity of the carbon source in determining algae-bacteria interactions.

One important observation from Figure 3 is that initial pH and buffering capacity are shown to affect algae-bacteria interactions. This result agrees with surveys of communities in the wild, which show that pH is an important environmental factor in determining community structure.[37–39] By contrast, most previous experimental interrogations of interactions between phototrophs and heterotrophs focus on the role of nutrient concentration and competition.[15,17–19,25] We expect that pH and buffering capacity are likely affecting interactions by influencing physiology, including nutrient uptake rates.

Next, we sought a framework to quantify the interaction between algae and bacteria in our experiment. We considered consumer-resource models to quantify competition for carbon, nitrogen, and phosphorus. However, the interactions in our community cannot be described by a model that considers only these nutrients. For example, the overall inhibition of *E. coli* does not depend in a simple way on the concentration of nutrients. Similarly, variations in pH are not naturally modeled in a consumer-resource framework. Hence, a simple consumer-resource model approach is not suitable for dissecting the interactions in our data. We, therefore, took a statistical approach using simple linear regressions to model interactions as a function of the environmental factors.

Quantifying algae-bacteria interactions statistically

Our goal is to quantify how the presence of algae or bacteria impacts the growth of the other species across all the environmental conditions tested. To do this, we developed a simple framework for estimating interactions in the algae-bacteria communities via regression analyses. Specifically, we used a linear regression formalism to predict algal or bacterial growth (Figure 2C) using environmental factors (pH, buffering capacity, phosphorus concentration, and carbon concentration) as independent variables. We designed a regression approach based on Monod's growth law (STAR Methods), which allowed us to estimate the role of environmental factors and the presence or absence of the other species on growth while retaining a high level of interpretability. We performed independent regressions to predict algal and bacterial growth across all conditions.

Our regression approach can be explained mathematically using a simple example. To do this, first consider communities of algae and bacteria where the total growth is affected by a single environmental factor (X) and by the presence of the other species via an interaction. Our regression was designed to measure the *change* in the growth of the target species (algae or bacteria) in response to changes in X. In this scenario, the model for predicting the growth of *E. coli* in monoculture and coculture takes the following form:

$$Y^{Ec} = \left(\beta^{Ec}_{1,M} + I\beta^{Ec}_{1,I}\right) + X\left(\beta^{Ec}_{X,M} + I\beta^{Ec}_{X,I}\right) \quad \text{(Equation 1)}$$

where Y^{Ec} is the growth of *E. coli* and the $\beta^{Ec}_{*,*}$ are regression coefficients. I is a variable that indicates the presence ($I = 1$) or absence ($I = 0$) of *C. reinhardtii*. The coefficient $\beta^{Ec}_{X,M}$ represents the change in growth in monoculture per unit change in X and $(\beta^{Ec}_{X,M} + \beta^{Ec}_{X,I})$ represents the change in growth in coculture per unit change in X (Figure 4A). Similarly, $\beta^{Ec}_{1,M}$ is the growth at $X = 0$ in monoculture and $\beta^{Ec}_{1,M} + I\beta^{Ec}_{1,I}$ is the growth at $X = 0$ in coculture. Hence, $\beta^{Ec}_{X,I}$, estimates the average change in growth per unit X in coculture relative to monoculture (Figure 4A, right). In other words, $\beta^{Ec}_{X,I}$ represents the effect of *C. reinhardtii* on *E. coli* as X increases in coculture. A positive coefficient would represent an enhancement of *E. coli* growth by *C. reinhardtii* as X increases (Figure 4B left). Similarly, a negative coefficient would represent suppression of *E. coli* growth by *C. reinhardtii* as X increases (Figure 4B, right). An identical regression is used to estimate the impact of *E. coli* on *C. reinhardtii* growth.

We extended the above model to include the effect of multiple environmental factors in determining the growth of both species (STAR Methods). For our dataset comprising of four environmental factors—initial pH (pH), buffering capacity (BC), phosphorus concentration ($[P]$), and carbon concentration ($[C]$), the model includes the following terms: $[P], [C], pH[P], pH[C], BC[P], BC[C], [P][C]$. For each term, we estimated a coefficient for monoculture and interaction as described above. For simplicity, we refer to coefficients of features without the indicator variable I as monoculture coefficients and coefficients of features with the indicator variable as interaction coefficients.

We did not include linear terms in pH or BC in our model because biologically pH alone does not generate biomass but instead modulates the ability of cells to grow on the available nutrients. Thus, we included only interaction effects between nutrients and pH or BC. Therefore, the coefficient $\beta^{Ec}_{pH[P]}$ represents the susceptibility of growth to phosphorus concentration modulated by pH. The feature $[P][C]$ was included to capture interactions between nutrients. Additionally, our model, being simple, cannot capture nonlinearities in the growth as a function of a

coculture. Note the fact that all points lie below this line, indicating the pervasive inhibition of bacteria by algae. The data in each panel are the same, but the colorbar represents each of the four environmental factors—initial pH (top left), buffering capacity (top right), phosphorus concentration (bottom left), and carbon concentration (bottom right). The colorbar for phosphorus is logarithmic. The carbon source is glycerol. See Figures S8 and S9 for the data in other carbon sources.

(B) Identical plots as in (A) but for algal growth in monoculture and coculture. The fact that most data lie near the dashed line indicates overall weaker impacts on algal growth by bacteria. Negative values of growth correspond to death where the number of cells detected declines from the beginning to the end of the experiment.

Please cite this article in press as: Gopalakrishnappa et al., Environmental modulators of algae-bacteria interactions at scale, Cell Systems (2024), https://doi.org/10.1016/j.cels.2024.08.002

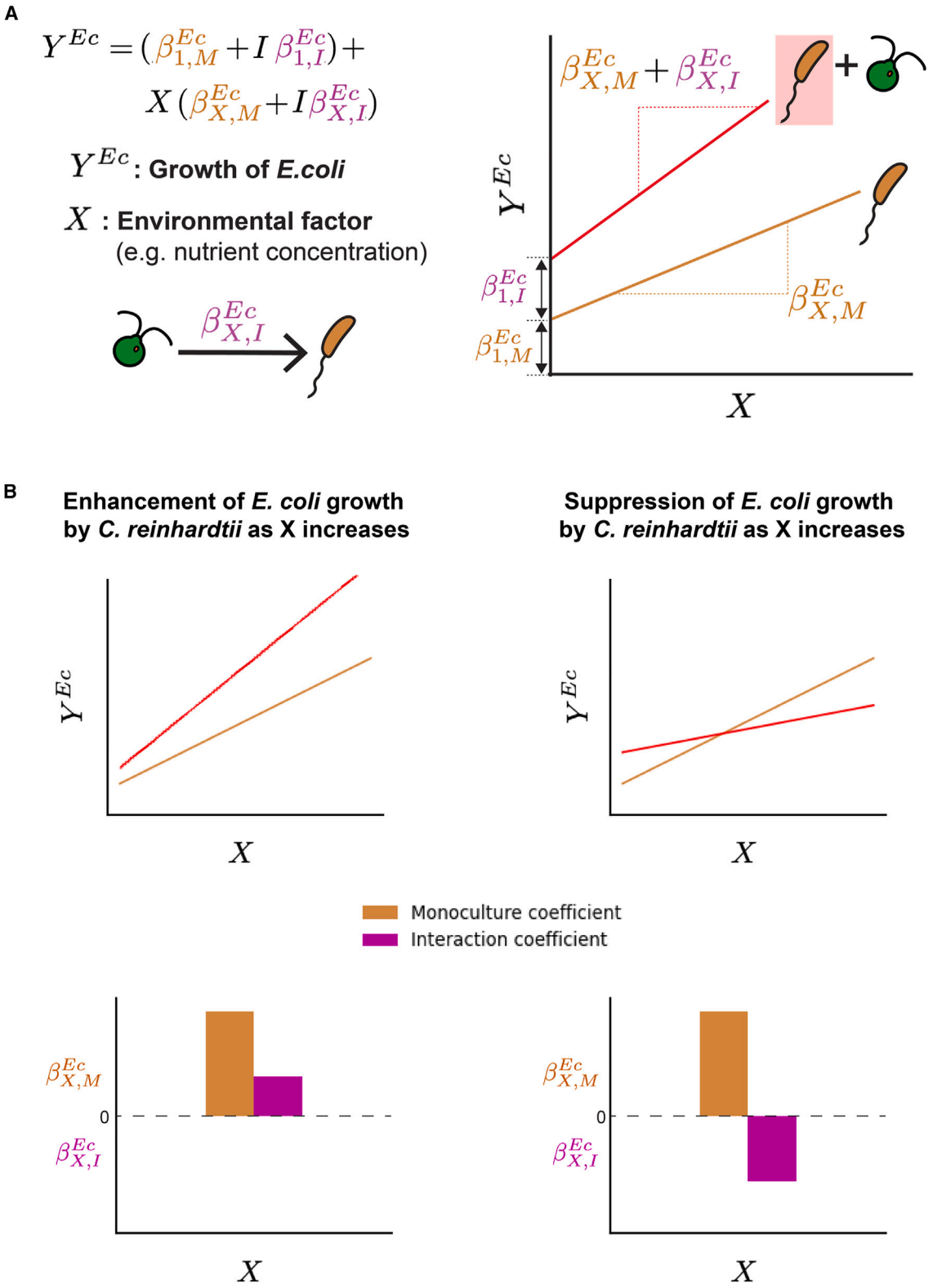

Figure 4. Quantifying algae-bacteria interactions via regression

(A) Formulation of the regression model for predicting growth from environmental conditions, here using *E. coli* as an example. Y^{Ec} is the growth of *E. coli* in monocultures and cocultures and X is an environmental factor that determines the growth. The indicator variable I is set to 0 for growth in monoculture and 1 for growth in coculture. The coefficient $\beta^{Ec}_{X,M}$ represents the change in growth in monoculture with X and is referred to as a monoculture coefficient. The coefficient

(legend continued on next page)

Please cite this article in press as: Gopalakrishnappa et al., Environmental modulators of algae-bacteria interactions at scale, Cell Systems (2024), https://doi.org/10.1016/j.cels.2024.08.002

nutrient concentration. Despite these limitations, this statistical approach allows us to achieve a unified and interpretable picture of interactions between these microbes across a wide range of environmental conditions.

Finally, to account for the fact that algae globally inhibit bacterial growth in our experiment, we standardize the growth of both *E. coli* and *C. reinhardtii* prior to performing the regression above (STAR Methods). Thus, our regressions describe variation in bacterial growth after removing the effect of this global inhibition. It is important to recognize that in no condition do the bacteria actually grow better in monoculture than in coculture (Figure 3A). To facilitate interpretation, we also standardized all the independent variables in the regression. As a result, the regression coefficients describe the relative change in growth per unit change in each environmental factor. This standardization also allows us to compare coefficient values for regressions performed on different carbon sources despite variation in the growth on those nutrients. To perform the regression, we fit the growth measured in each well using a weighted least-square approach (STAR Methods).

In general, we find that this model provides good predictions of growth across environmental conditions in our experiment, with the fits being better for some carbon sources (glucose, glycerol, and acetate) than others (galactose) (Figure S10). We successfully validated a few coefficients obtained from the regression model in microtiter plates (STAR Methods and Dataset 3; Figure S22). Further, we note that the buffering ability of the phosphorus source in our experiments did not significantly affect our regression results (STAR Methods). Lastly, we found that a more complex model, such as a decision tree regression, gives superb fits to the data at the expense of interpretability (Figures S15 and S16).

pH and buffering capacity modulate nutrient dependence of algae-bacteria interactions

Using the linear regression approach outlined above, we modeled the dependence of algal and bacterial growth on the environmental factors for each of the five carbon sources in monoculture and coculture. We first looked at the regression coefficients describing the growth of *E. coli* in one particular carbon source (glycerol, Figure 5A). Of all the monoculture coefficients (brown bars in top panel, Figure 5A) obtained from fitting *E. coli* growth in glycerol, the coefficient of $BC[C]$ is the largest, suggesting a strong interaction of buffering capacity with carbon concentration in determining the monoculture growth. Thus, when *BC* is high, there is a substantially higher growth per unit $[C]$ than when *BC* is low. These results are consistent with the greater acidification of the environment at lower buffering capacity observed in the microtiter plate experiments (STAR Methods); this greater acidification likely negatively impacts *E. coli*. Therefore, the *E. coli* growth is expected to be higher at a higher buffering capacity for the same carbon concentration, which is reflected in the high value of the $BC[C]$ coefficient. In addition to $BC[C]$, there also exist statistically significant interactions between pH and carbon concentration and buffering capacity and phosphorus concentration, with the magnitude of the coefficients of $pH[C]$ and $BC[P]$ being comparable or greater than the coefficients of $[P]$ and $[C]$ alone. Mechanistically interpreting each of these coefficients is beyond the scope of this work but could be pursued via additional experiments in the droplet platform or lower throughput batch cultures.

Next, among the interaction coefficients containing the factors *pH* and *BC* (magenta bars in Figure 5A, top panel), the coefficients of $pH[C]$, $BC[P]$, and $BC[C]$ are non-zero and compare in magnitude with their respective monoculture coefficients. This reveals that the effects of $pH[C]$, $BC[P]$, and $BC[C]$, on bacterial growth in coculture are significantly different compared with their effects in monoculture. We conclude from this that the interaction between *C. reinhardtii* on *E. coli* is strongly impacted by pH and buffering capacity. This is a central finding of our study.

The fact that pH and buffering capacity of the environment can strongly influence interactions is illustrated by looking at a specific example from the data (Figure 5B). Choosing a subset of data corresponding to a specific phosphorus concentration ($[P] \sim 1.51$ mM), we compared the change in growth with carbon concentration in monocultures and cocultures at the different pH and buffering capacity values. The change in *E. coli* growth in monoculture with carbon concentration at the different buffering capacities shows different behavior (Figure 5B, left). Particularly, the increase in the growth with carbon concentration is observed to be higher in the condition with high buffering capacity (and low pH) compared with the increase in the condition with low buffering capacity (and high pH) as expected, with the trends in the model and the data being in good agreement. Next, we compare these results with *E. coli* growth in coculture. The trends in *E. coli* growth with carbon concentration in coculture is distinct from monoculture and depends on the pH and buffering capacity values (Figure 5B right). The growth appreciably declines with carbon concentration in the condition with low pH (and high buffering capacity), whereas there is an increase in growth with carbon concentration at high pH (and low buffering capacity), with the model reasonably capturing the trend in the data. These results agree with the positive coefficient of $pH[C]$ and ~ 0 coefficient of $BC[C]$ obtained when the model is evaluated for *E. coli* growth in coculture (sum of brown and magenta $pH[C]$ and $BC[C]$ bars in Figure 5A top panel and S13A).

In terms of interactions between *E. coli* and *C. reinhardtii*, the result can be summarized as follows: although an enhancement of *E. coli* growth is observed as carbon concentration increases in monoculture, the effect on *E. coli* by *C. reinhardtii* in coculture as carbon concentration increases is inhibitory at low pH and high buffering capacity but facilitatory at high pH and low buffering capacity (evidenced by the positive interaction coefficient

$\beta^{Ec}_{X,M} + \beta^{Ec}_{X,I}$ represents the change in growth in coculture with *X* (shown schematically in the plot on the right). Hence, the coefficient $\beta^{Ec}_{X,I}$ represents the change in the effect of *X* on growth in coculture relative to monoculture. The coefficient $\beta^{Ec}_{X,I}$ is dubbed an interaction coefficient.

(B) Illustration of enhancement and suppression of *E. coli* growth by *C. reinhardtii* as *X* increases. The growth of *E. coli* in monoculture (in brown) and coculture (in red) vs. the environmental factor X plotted in the case of enhancement (top left) and suppression (top right) of *E. coli* growth by *C. reinhardtii* as *X* increases. The panels on the bottom row show the corresponding regression coefficients. The monoculture coefficient $\beta^{Ec}_{X,M}$ (in brown) and interaction coefficient $\beta^{Ec}_{X,I}$ (in magenta) in the case of enhancement (bottom left) and suppression (bottom right) of *E. coli* growth by *C. reinhardtii* as *X* increases.

Please cite this article in press as: Gopalakrishnappa et al., Environmental modulators of algae-bacteria interactions at scale, Cell Systems (2024), https://doi.org/10.1016/j.cels.2024.08.002

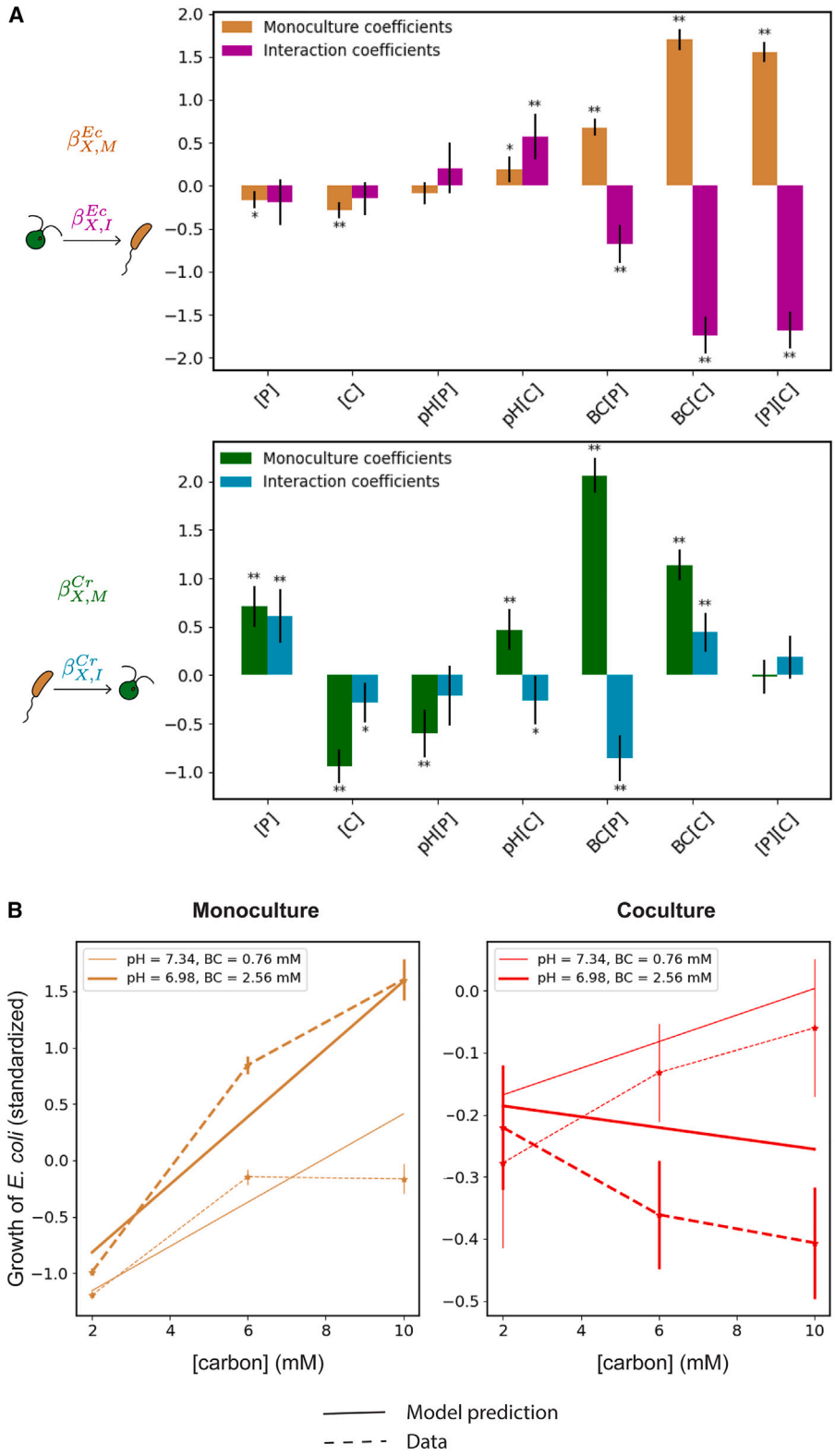

Figure 5. pH and buffering capacity modulate nutrient dependence of algae-bacteria interactions

(A) The coefficients for regressions predicting algal and bacterial growth in coculture and monoculture in glycerol. The results for the other carbon sources are shown in Figures S11 and S12. The top panel reports the monoculture coefficients $\beta^{Ec}_{X,M}$ (brown bars) and the interaction coefficients $\beta^{Ec}_{X,I}$ (magenta bars) of the corresponding features on the x axis obtained for the regression model predicting the growth of *E. coli* in monocultures and cocultures. The interaction

(legend continued on next page)

Please cite this article in press as: Gopalakrishnappa et al., Environmental modulators of algae-bacteria interactions at scale, Cell Systems (2024), https://doi.org/10.1016/j.cels.2024.08.002

of *pH*[*C*] and the negative interaction coefficient of *BC*[*C*] obtained from regressing *E. coli* growth; purple bars in Figure 5A, top panel). This example illustrates that *C. reinhardtii* modulates the capacity of *E. coli* growth on carbon in a manner that depends on pH and buffering capacity of the environment.

Algal abundance dynamics also depend strongly on pH and buffering capacity. The regression coefficients for predicting algal growth on glycerol in monoculture and coculture are shown in Figure 5A bottom panel. In this regression, we observe a similar interplay between pH and buffering capacity and nutrient concentration, i.e., the monoculture coefficients of *pH*[*P*], *pH*[*C*], *BC*[*P*], and *BC*[*C*] (green bars in the bottom panel [Figure 5B]) are all non-zero and statistically significant, showing the presence of a modulation effect of pH and buffering capacity on nutrient concentration in determining *C. reinhardtii* growth in monoculture. Here, again, the largest monoculture coefficient is for the *BC*[*P*] term, indicating an increase in the growth of *C. reinhardtii* with phosphorus concentration and buffering capacity. Although the growth of *C. reinhardtii* is known to increase with phosphorus concentration,[46] we speculate that the increased phosphorus uptake leads to increased N utilization (the N source here is ammonium). Ammonium utilization by algae causes acidification of the environment,[47] which is known to negatively affect the growth of *C. reinhardtii*.[48] Therefore, we reason that the environments with high buffering capacity potentially prevent this acidification and hence favor increased growth of *C. reinhardtii*, as reflected in the high coefficient of *BC*[*P*].

The modulation of algal growth by bacteria also depends on pH and buffering capacity in a fashion similar to what we observe with bacteria. For example, the interaction coefficients of pH[C], *BC*[*P*] , and *BC*[*C*] (cyan bars in the bottom panel of Figure 5B) being significant means that the impacts of *E. coli* on *C. reinhardtii* growth is altered by an interplay between both pH and buffering capacity and nutrient concentration. Even in other carbon sources, the impacts of *E. coli* on *C. reinhardtii* growth modified by both pH and buffering capacity are observed (Figures S12 and S14).

Overall, the result that the interactions between algae and bacteria are impacted by pH and buffering capacity through their differential impacts on nutrient dependence on monoculture and coculture growth holds across carbon sources (Figures S11 and S12).

Effect of environmental factors on algae-bacteria interactions depends on the identity of carbon source

Finally, we investigated whether the dependence of algae-bacteria interactions on the environmental factors—pH, buffering capacity, phosphorus concentration, and carbon concentration—is further modulated by the identity of the carbon source available in the communities. Between several carbon source pairs, we found some apparent differences in the effect of environmental factors on algae-bacteria growth. For example, differences in several of the monoculture and interaction coefficients (which quantify the effect of environmental factors on growth and interactions) between glucose and galactose are clearly observed (Figure 6A). Although the feature *BC*[*C*] has the highest effect in predicting *E. coli* growth in the case of glucose, *BC*[*P*] is the feature with the highest importance in the case of galactose. In addition, the effect of *BC*[*C*] in predicting the *E. coli* growth is the opposite between glucose and galactose. Additionally, for *E. coli*, the coefficients of [*P*] and [*C*] show different patterns in glucose and galactose, with generally negative coefficients in glucose and coefficients of opposing sign for monoculture and interaction coefficients in galactose. Qualitatively similar patterns are observed in coefficients describing algal growth (Figures S11, S12, and S17). These observations suggest that the identity of the carbon source modulates how environmental factors impact algae-bacteria interactions.

To interrogate these patterns further, we classified carbon sources based on their modulation of the effect of environmental factors on algae-bacteria growth. To do this, we computed correlations between the regression coefficients (which quantify the effect of environmental factors on growth and interactions) obtained for predicting algae-bacteria growth, between all pairs of carbon sources. We performed hierarchical clustering of the carbon sources based on the monoculture and interaction coefficients of [*P*], [*C*], *pH*[*P*], *pH*[*C*], *BC*[*P*], *BC*[*C*], and [*P*][*C*] obtained from the regressions for the carbon sources (STAR Methods). The correlation matrix computed for the hierarchical clustering showed that glycerol is most similar to glucose, galactose is most similar to pyruvate, and acetate has no strong correlation with any of the carbon sources (Figure 6B, left). Therefore, hierarchical clustering identified three clusters of carbon sources in our dataset, with glucose and glycerol forming one cluster, galactose and pyruvate forming another cluster, and acetate forming a cluster of its own (Figure 6B, right).

We wondered why these different carbon sources would have such divergent impacts on interactions. We first examined the metabolic pathways associated with these carbon sources but found no correlation between the nature of the carbon sources (glycolytic/gluconeogenic) and the observed clustering pattern in carbon sources. We then suspected that bacterial utilization of distinct carbon sources could have differing impacts on pH. To test this idea, we grew *E. coli* in plates with each of the five carbon sources and measured the final pH. We found that glucose and glycerol both showed large drops in pH, whereas

coefficients (magenta bars) indicate the effects of *C. reinhardtii* on *E. coli* growth with an increase in the corresponding features in coculture. The bottom panel reports the monoculture coefficients $\beta^{Cr}_{X,M}$ (green bars) and the interaction coefficients $\beta^{Cr}_{X,I}$ (cyan bars) of the corresponding features on the x axis obtained from the regression model predicting the growth of *C. reinhardtii* in monoculture and coculture. The interaction coefficients (cyan bars) indicate the effects of *E. coli* on *C. reinhardtii* growth with an increase in the corresponding features in coculture. The error bars represent the 95% confidence intervals. ** indicates a p value < 0.001 and * a p value < 0.05.

(B) Example data illustrating modulation of the effect of carbon concentration on the growth of *E. coli* by pH and buffering capacity. The median bacterial growth in monoculture and coculture are plotted as a function of carbon concentration at (P) ~1.51 mM in the left and right panels, respectively. The experimental data are represented by circles and connected with dashed lines. The error bars represent the standard error about the mean bacterial growth, with the number of replicates ranging from ~14–114 for the different conditions. The solid lines represent the model prediction. Darker or thicker lines represent the results at low pH (6.98) and high buffering capacity (2.56 mM), and lighter or thinner lines represent the results at high pH (7.34) and low buffering capacity (0.76 mM).

Please cite this article in press as: Gopalakrishnappa et al., Environmental modulators of algae-bacteria interactions at scale, Cell Systems (2024), https://doi.org/10.1016/j.cels.2024.08.002

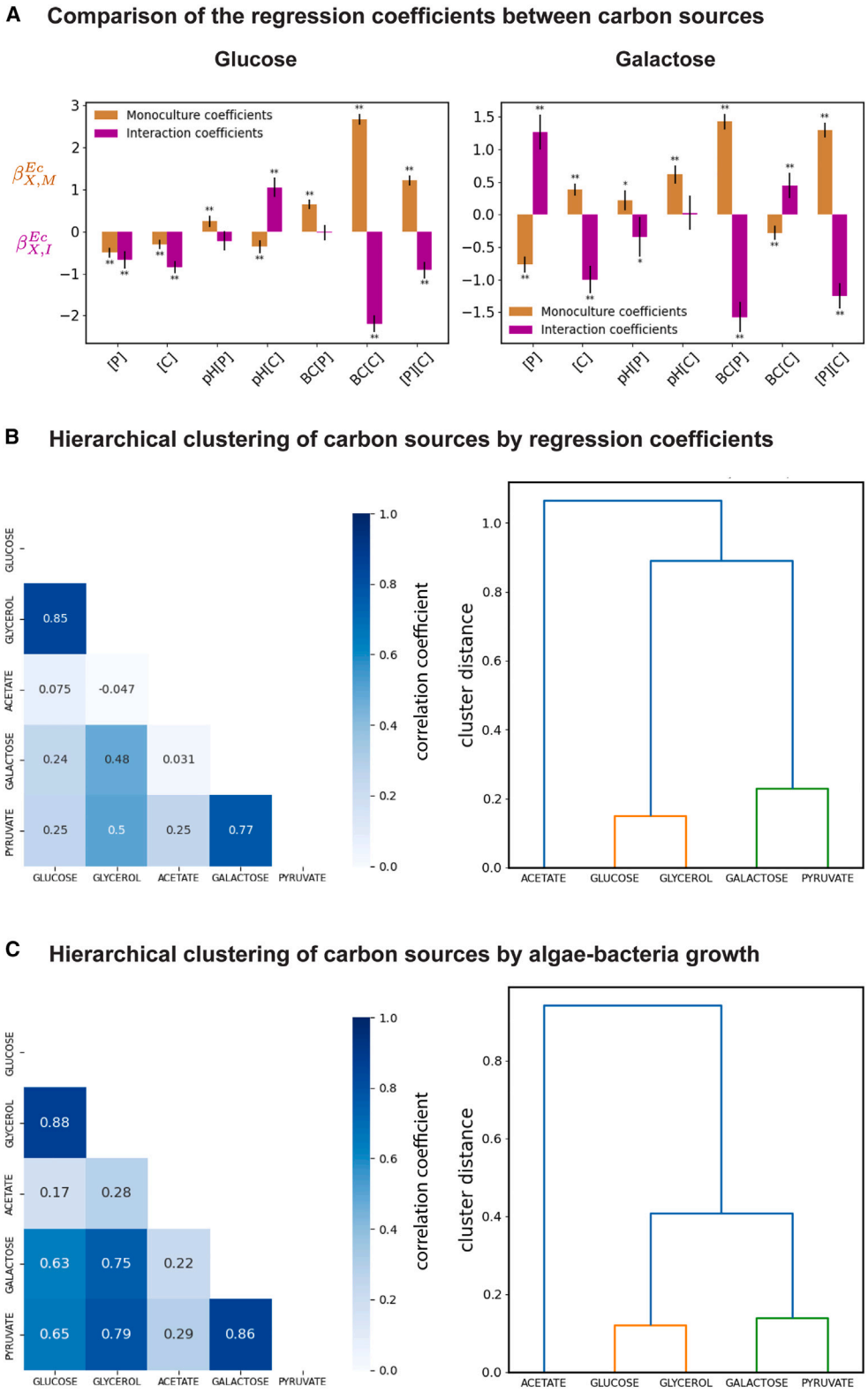

Figure 6. Effect of environmental factors on algae-bacteria interactions depends on the identity of carbon source

(A) Comparison of the regression coefficients between glucose and galactose. The monoculture coefficients $\beta^{Ec}_{X,M}$ (brown bars) and the interaction coefficients $\beta^{Ec}_{X,I}$ (magenta bars) of the corresponding features on the x axis obtained from the regression model predicting the growth of *E. coli* in monocultures and cocultures for glucose (on the left) and galactose (on the right). The error bars represent the 95% confidence intervals. ** indicates a p value < 0.001 and * a p value < 0.05.

(legend continued on next page)

Please cite this article in press as: Gopalakrishnappa et al., Environmental modulators of algae-bacteria interactions at scale, Cell Systems (2024), https://doi.org/10.1016/j.cels.2024.08.002

the other three carbon sources did not (STAR Methods). Thus, we speculate that heterotrophic utilization of organic carbon might play a key role in modulating pH and thus the interactions between algae and bacteria.

Finally, we wanted to check whether this result was dependent on the details of the regression formalism we defined for quantifying growth across environments. To do this, we quantified similarities in growth across environments in a model-independent fashion. We classified carbon sources based on the similarity in algae-bacteria growth. The classification of the carbon sources was done by computing the correlation between carbon sources in algae-bacteria growth across all the environmental conditions and culture conditions (Figure 6C; STAR Methods). Here, again, we found the carbon sources within the same clusters—glycerol and glucose, galactose, and pyruvate, to have the greatest correlation in the algae-bacteria growth with each other compared with any other carbon sources. We concluded that this apparent clustering of carbon sources does not depend on the details of our model specification.

DISCUSSION

By using a high-throughput droplet microfluidic platform, we were able to perform a massively parallel screening of algae-bacteria interactions in several hundreds of environmental conditions varying in pH, buffering capacity, phosphorus availability, carbon availability, and carbon source identity. To our knowledge, this is the largest screen exploring the combinatorial effect of environmental factors on phototroph-heterotroph interactions in a systematic way via a bottom-up approach. Studies in the past have tested for the effect of nutrient availability on phototroph-heterotroph relationships but have been mostly limited to only a handful of nutrient types/availabilities or have involved uncontrolled experimental conditions, such as uncharacterized phototrophic and heterotrophic species, often in the presence of organisms from other trophic levels.[15,19,49,50] Our observation of the complex dependence of algae-bacteria interactions on environmental factors underscores the importance of undertaking such high-dimensional studies. This is especially important in light of the chemical complexity of environments wild microbial communities are exposed to.[9]

Our study is also novel with respect to exploring the effect of the chemical properties of the environment—pH and buffering capacity—on algae-bacteria interactions. The central finding of the study is that pH and buffering capacity substantially alter algae-bacteria interactions by manipulating the impact of nutrient availabilities on growth. For most carbon sources, the role of pH and buffering capacity in determining algae-bacteria interactions were comparable to, or significantly higher than, the effect of nutrient availabilities alone, underscoring the importance of the effects of pH and buffering capacity on algae-bacteria interactions. This result suggests that chemical factors in the environments play an important role in impacting phototroph-heterotroph interactions, which are largely considered as being driven by resource exchange and competition.[15–17,19,22,25,36]

In the context of photosynthetic metabolism, pH, buffering capacity, and alkalinity are known to be important factors impacting the availability of inorganic carbon in the environment and the physiology of autotrophs. Changes in pH alter the equilibrium between CO_2 and bicarbonate, both of which can be taken up by the alga.[51,52] In addition, photosynthesis alters the pH of the environment via the utilization of inorganic carbon,[53] but this effect on pH can be altered by the presence of organic carbon at high concentrations (>100 mM) in the environment.[54] Similar to bacteria, algal growth is also inhibited by large changes in pH.[55] These observations are consistent with our regressions in that we find the buffering capacity to support significant and positive regression coefficients in monoculture for algae across carbon sources assayed (Figure S14). Thus, buffered media enable more robust algal growth presumably by enabling resistance to changes in pH driven by photosynthetic activity in the absence of bacteria.

Recently, microbial ecologists have encouraged the use of statistical modeling approaches to derive general governing principles in ecology.[56,57] In this regard, we highlight the apparent agreement between the results of our statistical modeling and the known mechanistic processes in literature. Our statistical approach for predicting algae-bacteria growth in different environments permitted us to dissect the contribution of the different environmental factors on the interspecies interactions. Although our modeling approach is largely agnostic to the detailed mechanisms of the effect of environmental factors on algae-bacteria interactions, we find that the regression results do align qualitatively with some known processes. For example, *E. coli* can acidify its environment when growing on glycolytic substrates at sufficiently high growth rates through the process of overflow metabolism.[58] In this case, the bacterium could be acidifying the medium in conditions where buffering capacity is weak, and carbon levels are relatively high. However, overflow occurs at relatively high growth rates of approximately 0.71/h–0.81/h, and microtiter measurements indicate that our strain in these conditions grows slower than this (STAR Methods, Table S5). Further, our measurements cannot accurately capture bacterial growth rates in droplets due to limited temporal sampling, but we cannot rule out the possibility that overflow causes growth to modify pH in the droplets. Similarly, it is known that *C. reinhardtii* will acidify the environment due to ammonia uptake, and this may also play a role in the importance of pH and buffering capacity in determining growth in these experiments. It remains an important avenue for future work to uncover the mechanisms underlying the interactions discovered here. Our

(B) Hierarchical clustering of carbon sources by the monoculture and interaction coefficients obtained from the regression models predicting the growth of *E. coli* and *C. reinhardtii*. The matrix showing correlations between the regression coefficients of the different carbon sources on the left and the resulting dendrogram from hierarchical clustering based on the correlation matrix on the right (see STAR Methods). The colors in the heatmap correspond to the correlation values indicated by the color bar in linear scale on the right.

(C) Hierarchical clustering of carbon sources by the median growth of algae and bacteria in monocultures and cocultures in all the environmental conditions. The correlation matrix computed for the hierarchical clustering on the left and the resulting dendrogram on the right (see STAR Methods). The colors in the heatmap correspond to the correlation values indicated by the color bar in linear scale, on the right.

Please cite this article in press as: Gopalakrishnappa et al., Environmental modulators of algae-bacteria interactions at scale, Cell Systems (2024), https://doi.org/10.1016/j.cels.2024.08.002

hope is that large-scale screens similar to those enabled by this platform can contribute new insights into the mechanisms by which environmental factors contribute to algae-bacteria interactions.

Our observation that interactions tend to favor competition (facilitation) in permissive (stressful) conditions is one example of how large-scale screens can help to identify general patterns in interactions. This observation (Figure 3) generally supports the SGH.[59] Earlier efforts to validate the SGH within the realm of plants and microbes underscore the difficulties linked to the inherent ambiguity of the hypothesis.[60] Specifically, it is evident that not all stressors seem to favor facilitative interactions.[61] Moreover, in instances where the SGH has been identified,[62] uncertainties persist regarding the existence of any shared underlying mechanisms. Our study points to the possibility that common environmental factors, such as pH or buffering capacity, might give rise to persistent patterns in interactions across environments. Validating this proposal would require additional measurements and physiological insights into the origins of the observed pattern.

Our exploration of the impact of carbon source identity on algae-bacteria interactions showed that the effect of the environmental factors—pH, buffering capacity, and nutrient availability—on the interspecies interactions depends on the carbon source identity. This result suggests that the chemical identity of the available reduced organic carbon plays a key role in determining how algae-bacteria interactions play out. Therefore, considering the role of individual nutrients such as phosphorus[63] in these interactions might be too simple a picture. Additionally, our analyses revealed three groups of carbon sources, showing that the impact of the environmental factors—pH, buffering capacity, and nutrient availability—on algae-bacteria interactions was approximately conserved between the carbon sources within the same group. Such an apparent similarity between the different carbon sources within the groups hints that there may be some relatively simple structure in how the carbon source identity and the other environmental factors conspire to determine the outcome of an interaction. Whether this is the case or not awaits a broader survey of additional carbon sources, mixtures of carbon sources, and a deeper mechanistic understanding of the physiology underlying these processes.

Although kChip offers a massive throughput advantage to perform a screen of this magnitude, the interactions inferred in the confined environments of droplets on the kChip could potentially differ from the interactions in the well-mixed, open environments in the lab or the wild. For example, the rate of gas exchange, particularly O_2 and CO_2, will determine respiration, photosynthesis, and pH and thereby modulate interactions in the droplets. In fact, a recent microfluidic-based study has shown that droplet size substantially modifies the degree of syntrophic interaction between bacterial species.[64] Consistent with these findings, we observe differences in bacterial growth between microtiter plates and droplets (Figure S18). Hence, it remains an important avenue for future work to understand how confinement impacts the algae-bacteria interactions observed here because this process could well be important in the wild.

Because our study of phototroph-heterotroph interactions was undertaken in a community of algae and bacteria that are not known to associate in the wild, it remains to be seen how our results relate to communities of phototroph and heterotroph with wild associations and shared evolutionary history. For example, the mechanism by which *C. reinhardtii* inhibits *E. coli* growth is not precisely known, and it is unclear whether other bacterial taxa would also be subjected to similar strong inhibitory effects. Studies between several strains of the phototroph, *Prochlorococcus*, and of oligotrophic and copiotrophic bacteria have revealed strain-dependent interactions.[65,66] Thus, it would be interesting to repeat these experiments with a broader sampling of bacterial taxa, including those that are known to associate with the alga in the wild.[67] By expanding this study to wild associations, we would hope to more broadly capture the relevance of these findings for consortia in complex environments.

RESOURCE AVAILABILITY

Lead contact

Further information and requests for resources and reagents should be directed to and will be fulfilled by the lead contact, Seppe Kuehn (seppe.kuehn@gmail.com).

Materials availability

This study did not generate new unique reagents.

Data and code availability

- Microscopy data and other datasets reported here are publicly available. DOIs are listed in the key resources table.
- All code required to reproduce the analyses has been deposited at Zenodo and is publicly available. DOIs are listed in the key resources table.
- Any additional information required to reanalyze the data reported in this paper is available from the lead contact upon request.

ACKNOWLEDGMENTS

We thank Jared Kehe, Anthony Kulesa, other members of the Blainey lab, and Amichai Baichman-Kass for helping set up the kChip system in our lab. We thank members of the Kuehn lab for helpful discussions. We also thank Austin Cyphersmith and the other core facilities staff at Carl R. Woese Institute for Genomic Biology for technical assistance with microscopy. This research was supported by the NSF MCB 2117477, Gordon and Betty Moore Foundation (GBMF 5263), Research Corporation Scialog Molecules Come to Life program, and CompGen fellowship from the University of Illinois at Urbana-Champaign. S.K. acknowledges support from the National Institutes of General Medical Science (RO1GM151538) and support from the National Science Foundation through the Center for Living Systems (grant no. 2317138).

AUTHOR CONTRIBUTIONS

C.G. and S.K. designed research. C.G. performed experiments. C.G. and S.K. analyzed data. Z.L. developed the model to predict pH and buffering capacity of the different environmental conditions. and C.G., Z.L., and S.K. wrote the paper.

DECLARATION OF INTERESTS

C.G. is currently employed by the Department of Civil and Environmental Engineering, Massachusetts Institute of Technology. Z.L. is currently employed by BillionToOne Inc.

DECLARATION OF GENERATIVE AI AND AI-ASSISTED TECHNOLOGIES IN THE WRITING PROCESS

During the preparation of this work the authors used Grammarly and ChatGPT to proof and improve readability. After using these tools/services, the authors

reviewed and edited the content as needed and take full responsibility for the content of the publication.

STAR★METHODS

Detailed methods are provided in the online version of this paper and include the following:

- KEY RESOURCES TABLE
- EXPERIMENTAL MODEL AND SUBJECT DETAILS
  - Strains
  - Plasmid transformation
  - Media
  - Culturing and harvesting of the microbes for kChip experiments
- METHOD DETAILS
  - Setting up the experiments on kChip
  - Image processing and analysis
  - Determining initial pH and buffering capacity of the environments on the kChip
  - Linear regression analyses
  - Computing coculture coefficients
- QUANTIFICATION AND STATISTICAL ANALYSIS
  - Estimating abundances of algae and bacteria
  - Estimating single-cell intensities
  - Obtaining abundances of algae and bacteria

SUPPLEMENTAL INFORMATION

Supplemental information can be found online at https://doi.org/10.1016/j.cels.2024.08.002.

Received: April 3, 2023
Revised: November 29, 2023
Accepted: August 7, 2024
Published: September 4, 2024

REFERENCES

1. Mickalide, H., and Kuehn, S. (2019). Higher-Order Interaction between Species Inhibits Bacterial Invasion of a Phototroph-Predator Microbial Community. Cell Syst. *9*, 521–533.e10. https://doi.org/10.1016/j.cels.2019.11.004.
2. Thompson, A.W., Foster, R.A., Krupke, A., Carter, B.J., Musat, N., Vaulot, D., Kuypers, M.M.M., and Zehr, J.P. (2012). Unicellular cyanobacterium symbiotic with a single-celled eukaryotic alga. Science *337*, 1546–1550. https://doi.org/10.1126/science.1222700.
3. Blanton, L.V., Charbonneau, M.R., Salih, T., Barratt, M.J., Venkatesh, S., Ilkaveya, O., Subramanian, S., Manary, M.J., Trehan, I., Jorgensen, J.M., et al. (2016). Gut bacteria that prevent growth impairments transmitted by microbiota from malnourished children. Science *351*, aad3311. https://doi.org/10.1126/science.aad3311.
4. Ratzke, C., and Gore, J. (2018). Modifying and reacting to the environmental pH can drive bacterial interactions. PLoS Biol. *16*, e2004248. https://doi.org/10.1371/journal.pbio.2004248.
5. Ilhan, Z.E., Marcus, A.K., Kang, D.-W., Rittmann, B.E., and Krajmalnik-Brown, R. (2017). pH-Mediated Microbial and Metabolic Interactions in Fecal Enrichment Cultures. mSphere *2*, e00047–17. https://doi.org/10.1128/mSphere.00047-17.
6. Hoek, T.A., Axelrod, K., Biancalani, T., Yurtsev, E.A., Liu, J., and Gore, J. (2016). Resource Availability Modulates the Cooperative and Competitive Nature of a Microbial Cross-Feeding Mutualism. PLoS Biol. *14*, e1002540. https://doi.org/10.1371/journal.pbio.1002540.
7. Burman, E., and Bengtsson-Palme, J. (2021). Microbial Community Interactions Are Sensitive to Small Changes in Temperature. Front. Microbiol. *12*, 672910. https://doi.org/10.3389/fmicb.2021.672910.
8. Whitney, J.C., Peterson, S.B., Kim, J., Pazos, M., Verster, A.J., Radey, M.C., Kulasekara, H.D., Ching, M.Q., Bullen, N.P., Bryant, D., et al. (2017). A broadly distributed toxin family mediates contact-dependent antagonism between gram-positive bacteria. eLife *6*, e26938. https://doi.org/10.7554/eLife.26938.
9. Kellerman, A.M., Dittmar, T., Kothawala, D.N., and Tranvik, L.J. (2014). Chemodiversity of dissolved organic matter in lakes driven by climate and hydrology. Nat. Commun. *5*, 3804. https://doi.org/10.1038/ncomms4804.
10. Kulesa, A., Kehe, J., Hurtado, J.E., Tawde, P., and Blainey, P.C. (2018). Combinatorial drug discovery in nanoliter droplets. Proc. Natl. Acad. Sci. USA *115*, 6685–6690. https://doi.org/10.1073/pnas.1802233115.
11. Seymour, J.R., Amin, S.A., Raina, J.-B., and Stocker, R. (2017). Zooming in on the phycosphere: the ecological interface for phytoplankton–bacteria relationships. Nat. Microbiol. *2*, 17065. https://doi.org/10.1038/nmicrobiol.2017.65.
12. Ramanan, R., Kim, B.-H., Cho, D.-H., Oh, H.-M., and Kim, H.-S. (2016). Algae–bacteria interactions: Evolution, ecology and emerging applications. Biotechnol. Adv. *34*, 14–29. https://doi.org/10.1016/j.biotechadv.2015.12.003.
13. Segev, E., Wyche, T.P., Kim, K.H., Petersen, J., Ellebrandt, C., Vlamakis, H., Barteneva, N., Paulson, J.N., Chai, L., Clardy, J., and Kolter, R. (2016). Dynamic metabolic exchange governs a marine algal-bacterial interaction. eLife *5*, e17473. https://doi.org/10.7554/eLife.17473.
14. Kritzberg, E.S., Cole, J.J., Pace, M.L., Granéli, W., and Bade, D.L. (2004). Autochthonous versus allochthonous carbon sources of bacteria: results from whole-lake 13C addition experiments. Limnol. Oceanogr. *49*, 588–596. https://doi.org/10.4319/lo.2004.49.2.0588.
15. Bratbak, G., and Thingstad, T.F. (1985). Phytoplankton-bacteria interactions: an apparent paradox? Analysis of a model system with both competition and commensalism. Mar. Ecol. Prog. Ser. *25*, 23–30. https://doi.org/10.3354/meps025023.
16. Zhang, Z., Nair, S., Tang, L., Zhao, H., Hu, Z., Chen, M., Zhang, Y., Kao, S.-J., Jiao, N., and Zhang, Y. (2021). Long-Term Survival of Synechococcus and Heterotrophic Bacteria without External Nutrient Supply after Changes in Their Relationship from Antagonism to Mutualism. mBio *12*, e0161421. https://doi.org/10.1128/mBio.01614-21.
17. Roberts, B.J., and Howarth, R.W. (2006). Nutrient and light availability regulate the relative contribution of autotrophs and heterotrophs to respiration in freshwater pelagic ecosystems. Limnol. Oceanogr. *51*, 288–298. https://doi.org/10.4319/lo.2006.51.1.0288.
18. Rier, S.T., and Stevenson, R.J. (2002). Effects of light, dissolved organic carbon, and inorganic nutrients on the relationship between algae and heterotrophic bacteria in stream periphyton. Hydrobiologia *489*, 179–184. https://doi.org/10.1023/A:1023284821485.
19. Rhee, G.-Y. (1972). Competition Between an Alga and an Aquatic Bacterium for Phosphate1. Limnol. Oceanogr. *17*, 505–514. https://doi.org/10.4319/lo.1972.17.4.0505.
20. Pope, C.A., Halvorson, H.M., Findlay, R.H., Francoeur, S.N., and Kuehn, K.A. (2020). Light and Temperature Mediate Algal Simulation of Heterotrophic Activity On Decomposing Leaf Litter. Freshw. Biol. *65*, 1210–1222. https://doi.org/10.1111/fwb.13465.
21. Mayers, T.J., Bramucci, A.R., Yakimovich, K.M., and Case, R.J. (2016). A Bacterial Pathogen Displaying Temperature-Enhanced Virulence of the Microalga Emiliania huxleyi. Front. Microbiol. *7*, 892. https://doi.org/10.3389/fmicb.2016.00892.
22. Lee, Y.-K., Ahn, C.-Y., Kim, H.-S., and Oh, H.-M. (2010). Cyanobactericidal effect of Rhodococcus sp. isolated from eutrophic lake on Microcystis sp. Biotechnol. Lett. *32*, 1673–1678. https://doi.org/10.1007/s10529-010-0350-5.
23. Cole, J.J. (1982). Interactions Between Bacteria and Algae in Aquatic Ecosystems. Annu. Rev. Ecol. Syst. *13*, 291–314. https://doi.org/10.1146/annurev.es.13.110182.001451.
24. Baines, S.B., and Pace, M.L. (1991). The production of dissolved organic matter by phytoplankton and its importance to bacteria: Patterns across

marine and freshwater systems. Limnol. Oceanogr. *36*, 1078–1090. https://doi.org/10.4319/lo.1991.36.6.1078.

25. Christie-Oleza, J.A., Sousoni, D., Lloyd, M., Armengaud, J., and Scanlan, D.J. (2017). Nutrient recycling facilitates long-term stability of marine microbial phototroph–heterotroph interactions. Nat. Microbiol. *2*, 17100. https://doi.org/10.1038/nmicrobiol.2017.100.
26. Grossart, H.-P., and Simon, M. (2007). Interactions of planktonic algae and bacteria: efects on algal growth and organic matter dynamics. Aquat. Microb. Ecol. *47*, 163–176. https://doi.org/10.3354/ame047163.
27. Prabhakara, K.H., and Kuehn, S. (2023). Algae drive convergent bacterial community assembly at low dilution frequency. iScience *26*, 106879. https://doi.org/10.1016/j.isci.2023.106879.
28. Tenorio, R., Fedders, A.C., Strathmann, T.J., and Guest, J.S. (2017). Impact of growth phases on photochemically produced reactive species in the extracellular matrix of algal cultivation systems. Environ. Sci.: Water Res. Technol. *3*, 1095–1108. https://doi.org/10.1039/C7EW00172J.
29. Sack, L., Zeyl, C., Bell, G., Sharbel, T., Reboud, X., Bernhardt, T., and Koelewyn, H. (1994). Isolation of four new strains of *Chlamydomonas reinhardtii* chlorophyta from soils samples. J. Phycol. *30*, 770–773. https://doi.org/10.1111/j.0022-3646.1994.00770.x.
30. Ishii, S., Ksoll, W.B., Hicks, R.E., and Sadowsky, M.J. (2006). Presence and growth of naturalized Escherichia coli in temperate soils from lake superior watersheds. Appl. Environ. Microbiol. *72*, 612–621. https://doi.org/10.1128/AEM.72.1.612-621.2006.
31. Savageau, M.A. (1983). Escherichia coli Habitats, Cell Types, and Molecular Mechanisms of Gene Control. Am. Nat. *122*, 732–744. https://doi.org/10.1086/284168.
32. Frentz, Z., Kuehn, S., and Leibler, S. (2015). Strongly Deterministic Population Dynamics in Closed Microbial Communities. Phys. Rev. X *5*, 041014. https://doi.org/10.1103/PhysRevX.5.041014.
33. Hekstra, D.R., and Leibler, S. (2012). Contingency and Statistical Laws in Replicate Microbial Closed Ecosystems. Cell *149*, 1164–1173. https://doi.org/10.1016/j.cell.2012.03.040.
34. Gąsiorowski, M., Stienss, J., Sienkiewicz, E., and Sekudewicz, I. (2021). Geochemical Variability of Surface Sediment in Post-Mining Lakes Located in the Muskau Arch (Poland) and Its Relation to Water Chemistry. Water Air Soil Pollut. *232*, 108. https://doi.org/10.1007/s11270-021-05057-8.
35. Grochowska, J. (2020). Assessment of Water Buffer Capacity of Two Morphometrically Different, Degraded, Urban Lakes. Water *12*, 1512. https://doi.org/10.3390/w12051512.
36. González, J.M., Simó, R., Massana, R., Covert, J.S., Casamayor, E.O., Pedrós-Alió, C., and Moran, M.A. (2000). Bacterial community structure associated with a dimethylsulfoniopropionate-producing North Atlantic algal bloom. Applied and environmental microbiology *66*, 4237.
37. Hartman, W.H., Richardson, C.J., Vilgalys, R., and Bruland, G.L. (2008). Environmental and anthropogenic controls over bacterial communities in wetland soils. Proc. Natl. Acad. Sci. USA *105*, 17842–17847. https://doi.org/10.1073/pnas.0808254105.
38. Fierer, N., Morse, J.L., Berthrong, S.T., Bernhardt, E.S., and Jackson, R.B. (2007). Environmental controls on the landscape-scale biogeography of stream bacterial communities. Ecology *88*, 2162–2173. https://doi.org/10.1890/06-1746.1.
39. Crocker, K., Lee, K.K., Chakraverti-Wuerthwein, M., Li, Z., Tikhonov, M., Mani, M., Gowda, K., and Kuehn, S. (2023). Global patterns in gene content of soil microbiomes emerge from microbial interactions. Preprint at bioRxiv. https://doi.org/10.1101/2023.05.31.542950.
40. Milo, R., Jorgensen, P., Moran, U., Weber, G., and Springer, M. (2010). BioNumbers—the database of key numbers in molecular and cell biology. Nucleic Acids Res. *38*, D750–D753. https://doi.org/10.1093/nar/gkp889.
41. Aidelberg, G., Towbin, B.D., Rothschild, D., Dekel, E., Bren, A., and Alon, U. (2014). Hierarchy of non-glucose sugars in Escherichia coli. BMC Syst. Biol. *8*, 133. https://doi.org/10.1186/s12918-014-0133-z.
42. Kim, J., Cheong, Y.E., Jung, I., and Kim, K.H. (2019). Metabolomic and Transcriptomic Analyses of Escherichia coli for Efficient Fermentation of L-Fucose. Mar. Drugs *17*, 82. https://doi.org/10.3390/md17020082.
43. Kehe, J., Kulesa, A., Ortiz, A., Ackerman, C.M., Thakku, S.G., Sellers, D., Kuehn, S., Gore, J., Friedman, J., and Blainey, P.C. (2019). Massively parallel screening of synthetic microbial communities. Proc. Natl. Acad. Sci. USA *116*, 12804–12809. https://doi.org/10.1073/pnas.1900102116.
44. Kehe, J., Ortiz, A., Kulesa, A., Gore, J., Blainey, P.C., and Friedman, J. (2021). Positive interactions are common among culturable bacteria. Sci. Adv. *7*, eabi7159. https://doi.org/10.1126/sciadv.abi7159.
45. Baichman-Kass, A., Song, T., and Friedman, J. (2023). Competitive interactions between culturable bacteria are highly non-additive. eLife *12*, e83398. https://doi.org/10.7554/eLife.83398.
46. de Lello, N., Garha, J., Infanti, D., and Raj, J. (2019). Effect of phosphorus concentration on growth rate of Chlamydomonas reinhardtii. Expedition *9*.
47. Scherholz, M.L., and Curtis, W.R. (2013). Achieving pH control in microalgal cultures through fed-batch addition of stoichiometrically-balanced growth media. BMC Biotechnol. *13*, 39. https://doi.org/10.1186/1472-6750-13-39.
48. Grewal, G., Kim, R., and Mason-Newton, S. (2018). How does pH impact the growth of Chlamydomonas reinhardtii. Expedition *7*.
49. Diner, R.E., Schwenck, S.M., McCrow, J.P., Zheng, H., and Allen, A.E. (2016). Genetic Manipulation of Competition for Nitrate between Heterotrophic Bacteria and Diatoms. Front. Microbiol. *7*, 880. https://doi.org/10.3389/fmicb.2016.00880.
50. Burson, A., Stomp, M., Greenwell, E., Grosse, J., and Huisman, J. (2018). Competition for nutrients and light: testing advances in resource competition with a natural phytoplankton community. Ecology *99*, 1108–1118. https://doi.org/10.1002/ecy.2187.
51. Wang, Y., Duanmu, D., and Spalding, M.H. (2011). Carbon dioxide concentrating mechanism in Chlamydomonas reinhardtii: inorganic carbon transport and CO2 recapture. Photosynth. Res. *109*, 115–122. https://doi.org/10.1007/s11120-011-9643-3.
52. Wang, Y., Stessman, D.J., and Spalding, M.H. (2015). The CO2 concentrating mechanism and photosynthetic carbon assimilation in limiting CO2: how Chlamydomonas works against the gradient. Plant J. *82*, 429–448. https://doi.org/10.1111/tpj.12829.
53. Neumann, J., and Levine, R.P. (1971). Reversible pH Changes in Cells of Chlamydomonas reinhardi Resulting from CO2 Fixation in the Light and Its Evolution in the Dark 1. Plant Physiol. *47*, 700–704. https://doi.org/10.1104/pp.47.5.700.
54. Schuldiner, S., and Ohad, I. (1969). Biogenesis of chloroplast membranes. III. Light-dependent induction of proton pump activity in whole cells and its correlation to cytochrome f photo-oxidation during greening of a Chlamydomonas reinhardti mutant (y-1). Biochim. Biophys. Acta *180*, 165–177. https://doi.org/10.1016/0005-2728(69)90203-5.
55. Ochoa-Alfaro, A.E., Gaytán-Luna, D.E., González-Ortega, O., Zavala-Arias, K.G., Paz-Maldonado, L.M.T., Rocha-Uribe, A., and Soria-Guerra, R.E. (2019). pH effects on the lipid and fatty acids accumulation in Chlamydomonas reinhardtii. Biotechnol. Prog. *35*, e2891. https://doi.org/10.1002/btpr.2891.
56. Sanchez, A., Bajic, D., Diaz-Colunga, J., Skwara, A., Vila, J.C.C., and Kuehn, S. (2023). The community-function landscape of microbial consortia. Cell Syst. *14*, 122–134. https://doi.org/10.1016/j.cels.2022.12.011.
57. Gopalakrishnappa, C., Gowda, K., Prabhakara, K.H., and Kuehn, S. (2022). An ensemble approach to the structure-function problem in microbial communities. iScience *25*, 103761. https://doi.org/10.1016/j.isci.2022.103761.
58. Basan, M., Hui, S., Okano, H., Zhang, Z., Shen, Y., Williamson, J.R., and Hwa, T. (2015). Overflow metabolism in Escherichia coli results from efficient proteome allocation. Nature *528*, 99–104. https://doi.org/10.1038/nature15765.
59. Bertness, M.D., and Callaway, R. (1994). Positive interactions in communities. Trends Ecol. Evol. *9*, 187–191.

60. Hammarlund, S.P., and Harcombe, W.R. (2019). Refining the stress gradient hypothesis in a microbial community. Proc. Natl. Acad. Sci. USA *116*, 15760–15762. https://doi.org/10.1073/pnas.1910420116.

61. Maestre, F.T., Valladares, F., and Reynolds, J.F. (2005). Is the change of plant-plant interactions with abiotic stress predictable? A meta-analysis of field results in arid environments. J. Ecol. *93*, 748–757. https://doi.org/10.1111/j.1365-2745.2005.01017.x.

62. Piccardi, P., Vessman, B., and Mitri, S. (2019). Toxicity drives facilitation between 4 bacterial species. Proc. Natl. Acad. Sci. USA *116*, 15979–15984. https://doi.org/10.1073/pnas.1906172116.

63. Carpenter, S.R. (2008). Phosphorus control is critical to mitigating eutrophication. Proc. Natl. Acad. Sci. USA *105*, 11039–11040. https://doi.org/10.1073/pnas.0806112105.

64. Tan, J.Y., Saleski, T.E., and Lin, X.N. (2022). The effect of droplet size on syntrophic dynamics in droplet-enabled microbial co-cultivation. PLoS ONE *17*, e0266282. https://doi.org/10.1371/journal.pone.0266282.

65. Sher, D., Thompson, J.W., Kashtan, N., Croal, L., and Chisholm, S.W. (2011). Response of Prochlorococcus ecotypes to co-culture with diverse marine bacteria. ISME J. *5*, 1125–1132. https://doi.org/10.1038/ismej.2011.1.

66. Weissberg, O., Aharonovich, D., and Sher, D. (2023). Phototroph-heterotroph interactions during growth and long-term starvation across Prochlorococcus and Alteromonas diversity. ISME J. *17*, 227–237. https://doi.org/10.1038/s41396-022-01330-8.

67. Durán, P., Flores-Uribe, J., Wippel, K., Zhang, P., Guan, R., Melkonian, B., Melkonian, M., and Garrido-Oter, R. (2022). Shared features and reciprocal complementation of the Chlamydomonas and Arabidopsis microbiota. Nat. Commun. *13*, 406. https://doi.org/10.1038/s41467-022-28055-8.

68. Fraebel, D.T., Mickalide, H., Schnitkey, D., Merritt, J., Kuhlman, T.E., and Kuehn, S. (2017). Environment determines evolutionary trajectory in a constrained phenotypic space. eLife *6*, e24669. https://doi.org/10.7554/eLife.24669.

69. Lutz, R., and Bujard, H. (1997). Independent and Tight Regulation of Transcriptional Units in Escherichia Coli Via the LacR/O, the TetR/O and AraC/I1-I2 Regulatory Elements. Nucleic Acids Res. *25*, 1203–1210. https://doi.org/10.1093/nar/25.6.1203.

70. Taub, F.B., and Dollar, A.M. (1964). A Chlorella-Daphnia Food-Chain Study: The Design of a Compatible Chemically Defined Culture Medium 1, 2. Limnol. Oceanogr. *9*, 61–74. https://doi.org/10.4319/lo.1964.9.1.0061.

71. de Jesús Astacioa, L.M., Prabhakara, K.H., Li, Z., Mickalide, H., and Kuehn, S. (2021). Closed microbial communities self-organize to persistently cycle carbon. Proc. Natl. Acad. Sci. USA *118*, e2013564118.

72. Sánchez-Clemente, R., Guijo, M.I., Nogales, J., and Blasco, R. (2020). Carbon Source Influence on Extracellular pH Changes along Bacterial Cell-Growth. Genes *11*, 1292. https://doi.org/10.3390/genes11111292.

73. Kehe, J.S. (2020). Massively parallel combinatorial microbiology. PhD thesis (Massachusetts Institute of Technology). https://dspace.mit.edu/handle/1721.1/127886.

74. Rumble, J. (2022). CRC Handbook of Chemistry and Physics vol. 103 (CRC Press).

75. Altman, D.G., and Bland, J.M. (2011). How to obtain the P value from a confidence interval. BMJ *343*, d2304. https://doi.org/10.1136/bmj.d2304. https://www.bmj.com/content/343/bmj.d2304.

76. Mira, P., Yeh, P., and Hall, B.G. (2022). Estimating microbial population data from optical density. PLoS ONE *17*, e0276040. https://doi.org/10.1371/journal.pone.0276040.

77. Mäki, A.J., Peltokangas, M., Kreutzer, J., Auvinen, S., and Kallio, P. (2015). Modeling carbon dioxide transport in PDMS-based microfluidic cell culture devices. Chem. Eng. Sci. *137*, 515–524. https://doi.org/10.1016/j.ces.2015.06.065.

78. Kanehashi, S., Sato, T., Sato, S., and Nagai, K. (2012). Microstructure and Gas Diffusivity of Poly(dimethylsiloxane) Dense Membrane Using Molecular Dynamics (MD) Simulation. Trans. Mat. Res. Soc. Japan *37*, 439–442. https://doi.org/10.14723/tmrsj.37.439.

Please cite this article in press as: Gopalakrishnappa et al., Environmental modulators of algae-bacteria interactions at scale, Cell Systems (2024), https://doi.org/10.1016/j.cels.2024.08.002

STAR★METHODS

KEY RESOURCES TABLE

REAGENT or RESOURCE	SOURCE	IDENTIFIER
Bacterial and Virus Strains		
Escherichia coli MG1655-motile	Coli Genetic Stock Center (CGSC)	8237
Fluorescent dyes		
Alexa Fluor 555	ThermoFisher Scientific	A33080
Alexa Fluor 594	ThermoFisher Scientific	A33082
Alexa Fluor 647	ThermoFisher Scientific	A33084
Deposited Data		
Microscopy and other datasets reporting algal-bacterial abundances in different media conditions and the code to reproduce the analyses	This work	Zenodo Data: https://doi.org/10.5281/zenodo.12151777
Experimental Models: Organisms/Strains		
Chlamydomonas reinhardtii UTEX 2244	University of Texas culture collection of algae	2244
Other		
kChip droplet microfluidic platform	Kulesa et al.[10]	https://www.pnas.org/doi/abs/10.1073/pnas.1802233115

EXPERIMENTAL MODEL AND SUBJECT DETAILS

Strains

The heterotroph was a bacterium, *Escherichia coli*, strain MG1655 (Coli Genetic Stock Center (CGSC) #8237), which was transformed to constitutively express a green fluorescent protein (GFP) on a plasmid (protocol below). We used a fluorescent protein coded on a plasmid to increase fluorescence intensity per cell which we found to be too low for the imaging modalities used here when the protein was genomically integrated. The bacteria were cryogenically preserved at -80 °C. The phototroph in the study was an alga, *Chlamydomonas reinhardtii*, strain UTEX2244 obtained from the University of Texas Austin Culture Collection of Algae utex.org. Algae were cryogenically preserved in liquid nitrogen https://utex.org/pages/cryopreservation#liquid.

Plasmid transformation

The transformation of the wild type strain of *E. coli* MG1655,[68] to express GFP on a plasmid, was done to enable the measurement of bacterial abundances via fluorescence microscopy. Firstly, the plasmid for the transformation was extracted from the *E. coli* strain, DH10B pZA 1R GFP,[69] following the protocol in the GeneJET Plasmid Miniprep kit #K0503 for the low copy number plasmids. Following this, the transformation protocol involved the following steps:

Preparation of electrocompetent cells

The wild-type MG1655 cells were grown from frozen stocks in a 5 mL overnight culture of Lysogeny Broth (LB) at 30 °C in a shaker incubator. 1/2 mL of the overnight culture was added to a flask containing 30 mL of LB and grown at 30 °C with shaking at 200 RPM until the OD600 reached 0.5-0.7. The flask was removed and the culture was cooled by swirling in an ice water slurry for five minutes, then placed on ice for ten minutes. The culture was transferred to a pre-chilled centrifuge tube and pelleted by centrifugation (5 min, 5000 RPM) in a refrigerated centrifuge chilled to 4 °C. The supernatant was dumped and the cells were washed in 10 mL of ice-cold 10% glycerol. Pelleting was repeated in the same way and two more glycerol washes were performed, followed by a final resuspension in 200 μL. The cells were immediately placed on ice and kept cold until electroporation.

Electroporation of plasmid

100 μL of the prepared electrocompetent cells were mixed with 5 μL of the extracted plasmid mix in a pre-chilled microcentrifuge tube before being transferred to a pre-chilled 0.1 cm gap electroporation cuvette (USA Scientific) and electroporated at 2 kV in an Electroporator 2510 (Eppendorf). 1 mL of LB was immediately added and 1h outgrowth at 30 °C with shaking was allowed before plating on an LB + ampicillin plate, which was grown overnight at 30 °C. A colony from the plate was grown overnight (30 °C, shaking) in 5 mL of LB+ampicillin, and a frozen glycerol stock of MG1655+GFP was created from the culture.

Please cite this article in press as: Gopalakrishnappa et al., Environmental modulators of algae-bacteria interactions at scale, Cell Systems (2024), https://doi.org/10.1016/j.cels.2024.08.002

Media

Modified Taub medium and nutrient sources

Modified Taub formed the base media in our experiments. Taub media is a freshwater mimic media that was originally created to support co-cultures of *Daphnia pulex* and *Chlorella pyrenoidosa*.[70] Several previous studies of microbial ecosystems that used the 1/2X Taub media with undefined carbon and nitrogen sources (proteose peptone)[1,32,33] demonstrated the ability of both *E. coli* and *C. reinhardtii* to grow on Taub. However, to probe the effect of nutrient concentration and nutrient sources on algae-bacteria interactions, we required the media in our experiments to be chemically defined. Hence, the undefined Taub media was modified to include chemically defined carbon and nitrogen sources in place of the proteose peptone, similar to that in.[71] NH_4Cl formed the nitrogen source in all our experiments and one of the five sources - glucose, glycerol, galactose, acetate, and pyruvate formed the carbon source in our experiments. The phosphate source in the media was also replaced with an equal mix of potassium phosphate monobasic ($KH_2\ PO_4$) and potassium phosphate dibasic ($K_2\ HPO_4$) salts. Modified 1X Taub stock was first prepared by removing the small amount of phosphate that is traditionally present in 1X Taub solution. It was later supplemented with buffers and nutrient sources at different concentrations to generate the desired environmental conditions for the kChip experiments (discussed below). The chemical composition of the modified 1X Taub medium is shown in Table S1.

Preparation of environmental conditions for the kChip experiments

For each carbon source, 16 environmental conditions varying in initial pH, buffering capacity, phosphorus concentration, and carbon concentration were prepared. The values of the environmental factors were chosen to be in the biological range: 6.1-7.5 for initial pH, 0-3.5 mM for buffering capacity, 0.01 mM - 4 mM for phosphorus concentration, 2 mM - 10 mM for carbon concentration. The environmental conditions were also barcoded at the time of their preparation by adding the three fluorescent dyes Alexa Fluor 555 (Thermo- Fisher Scientific A33080), Alexa Fluor 594 (Thermo- Fisher Scientific A33082), and Alexa Fluor 647 (Thermo-Fisher Scientific A33084) such that each environmental condition gets a unique combination of the dyes with the total dye concentration always summing to 1 μM. The dye concentrations will be later used to infer the environmental conditions of the communities formed on the kChip as discussed in a further section. The initial pH, buffering capacity, and nutrient concentrations along with the dye concentration values of the 16 environments are reported in Table S2. Note that the reported pH and buffering capacity values are not the measured but estimated values from a model we developed and experimentally validated (details presented in a subsequent section). The dye fluorescence characteristics were not significantly altered by changing pH. Additionally, these values are reported for environments having glucose/glycerol/galactose as the carbon source. When acetate/pyruvate is the source of carbon in the environments, the pH and buffering capacity slightly differ from those reported here and are computed using our model. Depending upon the carbon source, the appropriate values of pH and buffering capacity are used in all the analyses.

To prepare the 16 environmental conditions, we first prepared the following sets of stock solutions -

1. Stock solutions of the base media 1X Taub:

B1 - The modified 1X Taub media with 0.11% w/v bovine serum albumin (BSA)

B2 - The modified 1X Taub media with 20 mM MOPS buffer and titrated to a pH of 6.95 with 0.11% w/v BSA

B3 - The modified 1X Taub media with 30 mM Tris buffer and titrated to a pH of 7.5 with 0.11% w/v BSA

(BSA is added to the media to improve retention of the fluorescent dyes in droplets on the kChip)

2. Stock solutions of carbon:

C1 - ~417 mM of glucose/glycerol/galactose/pyruvate/acetate by moles of carbon

C2 - ~67 mM stocks glucose/glycerol/galactose/pyruvate/acetate by moles of carbon

3. Stock solution of Nitrogen:

N1 - 50 mM of NH_4Cl stock

4. Stock solutions of Phosphate:

P1 - 50 mM of phosphate stock ($KH_2\ PO_4$ + $K_2\ HPO_4$ in 1:1 ratio by moles)

P2 - 1 mM of phosphate stock ($KH_2\ PO_4$ + $K_2\ HPO_4$ in 1:1 ratio by moles)

P3 - 0.12 mM of phosphate stock ($KH_2\ PO_4$ + $K_2\ HPO_4$ in 1:1 ratio by moles) titrated to a pH of 7.5

P4 - 12 mM of phosphate stock ($KH_2\ PO_4$ + $K_2\ HPO_4$ in 1:1 ratio by moles) titrated to a pH of 7.5

5. Stock solution of Alexa Fluor 555:

D1 - 25 μM of Alexa Fluor 555 dye

6. Stock solution of Alexa Fluor 594:

D2 - 25 μM of Alexa Fluor 594 dye

7. Stock solution of Alexa Fluor 647:

D3 - 25 μM of Alexa Fluor 647 dye

These stock solutions formed the key components in setting the various properties of the environmental conditions - initial pH, buffering capacity, nutrient concentrations, and barcodes. The prepared stock solutions were mixed in the desired ratios using a liquid handling robot Opentrons OT-2 to obtain the 16 environmental conditions. The stock solutions and their volumes used for making each of the 16 environments are reported in Table S3. 480 μL of each of the 16 environments were prepared such that we obtained the indicated concentrations of nutrients and dyes (in Table S2) when 10 μL of the *E. coli* and *C. reinhardtii* cells suspended in the modified 1X Taub media were later independently added to 240 μL of each of the environments. In the 480 μL of the environments,

Please cite this article in press as: Gopalakrishnappa et al., Environmental modulators of algae-bacteria interactions at scale, Cell Systems (2024), https://doi.org/10.1016/j.cels.2024.08.002

230 μL was composed of one of the three base media stock solutions - B1/B2/B3, and the rest of the 250 μL was made up of stock solutions of carbon, nitrogen, phosphorus, and the dyes, depending on the media type.

Specifically, in environments E1-E8 (Table S3), the modified and unbuffered 1X Taub media, B1, formed the 230 μL volume of the 480 μL. E4-E8 differed from E1-E4 in the phosphate stock used. While untitrated phosphate stocks P1 and P2 were used to get the desired phosphorus levels in E1-E4, the titrated phosphate stocks P3 and P4 were used to obtain the desired phosphorus levels in E4-E8. The use of the phosphate stocks P3 and P4 titrated to a pH of 7.5 (greater than ~7 - the ~ pH of the stocks P1 and P2) caused the environments E7 and E8 to have higher pH than E1-E4. And, in the environments, E9-E12 and E13-E16, the buffered 1X Taub media B2 (having the MOPS buffer) and B3 (having the Tris buffer) respectively formed the 230 μL volume of the 480 μL. The strong buffers- Tris and MOPS were chosen to obtain the environments E9-E16 with high buffering capacities (~3.5 mM). And the low initial pH of the environments E9-E12(~6.9) is due to the modified 1X Taub media buffered with MOPS and titrated to a low pH of 6.95. Similarly, the higher initial pH of the environments E9-E12 (~7.4) is due to the modified 1X Taub media buffered with Tris and titrated to a high pH of 7.5. The pKa values of MOPS and Tris (7.1 and 7.9 at 30 °C) make them ideal choices as buffering agents at low pH and high pH respectively. Lastly, as is reported in Table S2, we chose higher phosphorus levels (0.03-3 mM) for the lower buffering capacity environments E1-E8 but lower phosphorus levels (0.01-0.08 mM) for the environments E9-E16 which have higher buffering capacity. This was because the source of phosphorus in our experiments (i.e $KH_2PO_4 + K_2HPO_4$ in 1:1 ratio by moles) acts as both a nutrient and a buffer, for example, against the potential acidification of the environment arising from carbon metabolism by *E. coli*.[72] As a result, lower phosphorus levels were sufficient to give rise to appreciable growth of *E. coli* in monocultures in the high buffering capacity environments whereas higher phosphorus levels were required in the lower buffering environments to result in the similar growth of *E. coli* in its monocultures. Therefore, our choice of different phosphorus levels at the different buffering capacities allowed us to investigate differences in the algae-bacteria interactions between environments giving rise to similar growth of *E. coli*.

Culturing and harvesting of the microbes for kChip experiments

Culturing

Before beginning the experiment, the bacteria and algae were cultured separately in distinct media, with both microbes undergoing two growth cycles in their respective media.

Bacteria were cultured from a freezer stock in 5 mL lysogeny broth (LB) with ampicillin added at a concentration of 50 μg/mL to retain the plasmid. The culture was incubated at 30 °C (New Brunswick Scientific C24 Incubator-Shaker), shaking at 200 RPM for ~16 hrs. It was then passaged into fresh 5 mL LB + 50 μg/mL ampicillin at 2500X dilution and grown for ~24 hrs at 30 °C shaking at 200 RPM, before finally harvesting for the experiments.

The alga, *C. reinhardtii* was cultured in a 30 °C shaker-incubator (New Brunswick Scientific C24 Incubator-Shaker), shaking at 200 RPM with 68.5 μmol $m^{-2}s^{-1}$ illumination in 10 mL Tris-Acetate-Phosphate (TAP) media, inoculated directly from a freezer stock. TAP is a defined media with acetic acid as a carbon source https://www.chlamycollection.org/methods/media-recipes/tap-and-tris-minimal/. After ~4 days, the algal culture was passaged into fresh 20 mL of TAP media at 250X dilution and grown for ~ 3 days at 30 °C shaking at 200 RPM, before finally harvesting for the experiments.

Cultures preparation

Prior to setting up the experiment on kChip, the harvested microbial cultures were washed thrice into modified 1X Taub media.

1 mL of the MG1655 culture was centrifuged in an eppendorf at 3000 RPM (eppendorf centrifuge 5417R) for 5 mins. The supernatant was immediately discarded and the pellet was resuspended in 1 mL of fresh modified 1X Taub. This process was repeated thrice and OD590 of the final suspension was adjusted to obtain 0.005 in the droplets by diluting it with the modified 1X Taub media.

20 mL of the UTEX 2244 culture was also centrifuged thrice in 20 mL falcon tubes at 500 RCF for 10 mins. The culture was concentrated sequentially after every centrifugation from 20 mL to 7.5 mL to 2 mL. By further concentration or dilution, the OD750 of the final suspension was adjusted to obtain 0.145 in the droplets by diluting it with the modified 1X Taub media. The optical densities were measured using the BioTek Synergy HT microplate reader.

METHOD DETAILS

Setting up the experiments on kChip

Droplet preparation

The cultures of *E. coli* and *C. reinhardtii* that were washed into the modified 1X Taub media and with their ODs set were independently added to the 16 barcoded environments of one of the five carbon sources at 25X dilution. Each of the environments was thoroughly mixed using an electronic pipettor by pipetting up and down at least three times to ensure thorough mixing of the barcode dyes and the cells. 20 μL aliquots of these environments harboring the *E. coli* and *C. reinhardtii* cells independently were transferred to a Bio-Rad QX200 cartridge and were emulsified into ~20,000 1 nl droplets in fluorocarbon oil (3M Novec 7500) stabilized with 2% (w/v) fluorosurfactant (RAN Biotech 008 FluoroSurfactant). For each carbon source, there were 32 kinds of droplets - 16 environmental conditions each having cells of *E. coli* and *C. reinhardtii* separately.

Setting up the kChip platform

The generated droplets of all the 16 environmental conditions having cells were pooled together into a 1 mL Eppendorf and mixed by pipetting up and down with a 200 μL pipette. 180 μL of the pooled and mixed droplets were loaded into kChip(k=2) as described in [10]. kChip is made of PDMS and contains an array of ~25,000 microwells each of which can take two droplets (~130 μm in diameter).

Please cite this article in press as: Gopalakrishnappa et al., Environmental modulators of algae-bacteria interactions at scale, Cell Systems (2024), https://doi.org/10.1016/j.cels.2024.08.002

Briefly, the kChip was suspended in the chip loader made of acrylic, such that a ~300–500 μm flow space was created between the chip and a hydrophobic glass substrate. The flow space was filled with fluorous oil (3 mL 3M, 7500) prior to loading, followed by the addition of the droplet pool to the loading slot. By flushing the flow space with oil, the droplets were made to spread around in the flow space and enter the microwells due to buoyancy. Also, the loader was tilted to further facilitate the movement of the droplet foam within the flow space until the microwells were filled with droplets. The flow space was then again replenished with 3 mL of the fluorous oil. On the side, a fresh MicroAmp Optical Adhesive film (ThremoFisher #4311971) was laid out on the bench with its sticky side facing up and wetted with ~1 mL of the fluorous oil. The kChip was carefully lifted off the acrylic loader and sealed with the film by running the chip against the wetted film on the edge of the bench.

The kChip was then imaged to infer the barcode identities and the starting cell densities in the wells. Following this, the droplet pairs in the microwells were merged by running the tip of a corona treater (Model BD-20, Electro-Technic Products) over the sealed side of the chip for 10 seconds. The merging of the droplets resulted in the formation of monocultures and cocultures of algae and bacteria in all environmental combinations of the initial 16 environments. Overall, 3 culture types (*E. coli* monoculture, *C. reinhardtii* monoculture, *E. coli - C. reinhardtii* coculture) in 105 environments were generated upon droplet merging for each of the carbon sources, with the number of replicates ranging from 3 to 330 (The median number of replicates ranged from ~30-85 depending upon the culture type). The kChip was then transferred with its film side facing up and covered with a glass slide, into a Ziploc bag containing a moist towel to maintain high humidity and minimize evaporation. The entire setup was housed in an environmental chamber at 30 °C and illuminated with a bulb (Utilitech pro L9PAR20/LEDG5) at (68.5 μmol $m^{-2}s^{-1}$, measured with LED light meter PCE-LED 20). The kChip was imaged at 12 h, 21 h, 45 h, and 68 h from the time of the first scan. For each carbon source, a separate kChip experiment was set up.

Fluorescence Microscopy

A widefield fluorescence microscope (Axio Observer.Z1) with X-CITE 120 lamp (Excelitas Technologies #012-63000) as the light source for fluorescence imaging, was used to scan the kChip for barcodes and the growth of the microbes. Images were acquired with a 5X/0.16 NA objective (Zeiss EC Plan-Neofluar) with FOV (Field of view) of 2.47 × 2 mm, which required collecting 644 images to scan one full kChip area covering all the microwells. Images were collected by a camera (Axiocam 506 monochromatic) at a bit depth of 14 with 5×5 binning and at an exposure time of 50 ms. The following filter sets were used to detect the five fluorophores: Alexa Fluor 555: Semrock Brightline SpOr-B-CSC-ZERO; Alexa Fluor 594: Omega optical Excitation filter-XB102/Dichroic-XF2014/Emission filter-XF3028; Alexa Fluor 647: Semrock, Brightline Cy5-4040B-CSC-ZERO; GFP: Zeiss filter Set 38 HE; chlorophyll: Chroma Technology 31017. The lamp power was manually set to obtain ~71 mW with the Alexa Fluor 555 filter/~8 mW with the Alexa Fluor 594 filter/~27 mW with the Alexa Fluor 647 filter, measured at 540 nm/590 nm/630 nm respectively using a Thorlabs power meter (with power sensor S121B). In addition to the fluorescence images, brightfield images were also acquired with a TL Halogen lamp (set to 1.51 V) as the light source at an exposure of 1.1 ms. The duration of an entire scan was about 50 min.

Image processing and analysis

The tiled images acquired at each time point were stitched together to form a single image of the entire chip having all the microwells, using the stitching module in the Zeiss Zen blue image analysis software. Also, the stitched images across the time points were aligned by manually estimating the rotation and the shift in the chip at each time point with respect to the image acquired at the first time point, and correcting for them using the rotate and shift features in the zen software. The aligned images were then used for further processing and analyses in Python. First, the aligned images were computationally redivided and cropped in Python to obtain 644 tiles with 10% overlap as processing a single large image would require too much memory. From here on, the image analysis pipeline involved (a) Correcting for chlorophyll bleed-through in the A647 image (see below); (b) Inferring barcodes to identify the environmental conditions in the droplet pairs in each microwell using the three fluorescence dye signals; (c) estimating abundances of *E. coli* and *C. reinhardtii* in all the environmental conditions. All analyses were performed with either custom Python scripts, or code obtained from.[10,44,73]

Correcting for chlorophyll bleed-through in the Alexa Fluor 647 images

Inspection of the microscopy images of the fluorophores showed algal cells to appear in the images acquired with the Alexa 647 filter (Figure S1 (left panel)). This bleed-through of the chlorophyll signal into the Alexa Fluor 647 channel is due to the overlap between the fluorescence spectrum of the chlorophyll pigment and the Alexa fluor 647 dye. The chlorophyll signal bleed-through into the Alexa Fluor 647 images would corrupt the barcode clustering process (discussed in the next section), which is crucial for identifying the environmental conditions formed on the chip. A computational solution was developed to address this issue that involved the following steps:

1. Apply sobel transform (using scikit-image) to the Alexa 647 image to find the edges of the algal cells
2. Obtain the mask of the sobel transformed image to extract the edges of the algal cells.
3. Use a gaussian filter (with sigma = 1 pixel, in SciPy) to set the intensities of the pixels within the edges in the mask to greater than 0.
4. Set all the pixel intensities greater than 0 to NaN. This step would essentially set the intensity of all the pixels corresponding to the algal cells in the mask to NaN.
5. Multiply the mask obtained in step 4 with the original Alexa 647 image with the chlorophyll bleed-through and using a 2D interpolation scheme (interpolate.griddata in SciPy), estimate the intensity values of the pixels that were set to NaN. The Alexa 647 image obtained after this correction algorithm is free from the bright signal from the chlorophyll fluorescence (Figure S1 (right panel)).

Inferring barcodes to identify environmental conditions

Following the correction of Alexa 647 images for chlorophyll bleed-through, the three dye channel images were analyzed to detect the barcodes of the droplets in the wells of kChip and thereby infer the environmental conditions formed in the microwells. Similar to the pipeline in a previously published work,[10] the algorithm began with creating images by summing up the three dye channels images and then applying a circular hough transform (scikit-image) on the summed images to detect the circular droplets in the wells. Using the positions of the droplets reported by the hough transform, the three-color dye fluorescence intensities of each of the droplets were extracted. The fluorescence of a dye in a droplet was calculated as the median of the pixel values in the respective dye's image in a square of size 10 × 10 pixels at the droplet center, after locally subtracting for the background fluorescence intensities. The three dye channel images were also smoothed by applying a median filter (SciPy) with a kernel size of 8 pixels, prior to computing the dye fluorescence intensities. Obtaining the three-color fluorescence intensities of all the droplets in this manner, the intensities were projected to a 2-dimensional plane on the basis of the constraint that the intensities summed to a constant (as the sum of the dye concentrations is a constant equal to 1 μM). The clusters of droplets formed in the 2-dimensional plane based on the dye ratios were identified by bounding the data points with manually defined polygons (using matplotlib.path). Finally, using the apriori knowledge of fluorescence-dye-ratios to environmental conditions mapping (from while designing the environmental conditions and barcoding), the droplets/clusters were assigned to the environmental conditions. This knowledge of the droplet positions and their environmental conditions allowed inference of the environmental conditions of the communities formed in the different microwells after the merging of the droplets.

Determining initial pH and buffering capacity of the environments on the kChip

Model to predict titration curves

To infer the pH and buffering capacity of all the barcoded environments and the environments formed by merging of the droplets on kChip, we developed a model to predict the pH titration curve of any environment given the concentrations of the nutrients and buffers in it.

A solution's buffering capacity is its resilience to pH change from additional acid or base. To characterize the buffering behavior of a defined media, we calculate the titration curve, which relates the change in pH of a solution to additions of strong acid or base.

Consider a medium consists of *a* molar K_2HPO_4, *b* molar KH_2PO_4, *c* molar Tris, *d* molar MOPS, and *e* molar NH_4Cl, titrated by HCl. We denote the quantity of acid (*HCl*) added by *x*. The objective is to calculate pH as a function of *x*, given by

$$\left[H_2PO_4^-\right] + \left[HPO_4^{2-}\right] = a + b \quad \text{(Equation 2)}$$

$$[Tris] + [TrisH^+] = c \quad \text{(Equation 3)}$$

$$[MOPS] + [MOPS^-] = d \quad \text{(Equation 4)}$$

$$[NH_3] + \left[NH_4^+\right] = e \quad \text{(Equation 5)}$$

$$\frac{\left[HPO_4^{2-}\right][H^+]}{\left[H_2PO_4^-\right]} = K_1 \quad \text{(Equation 6)}$$

$$\frac{[Tris][H^+]}{[TrisH^+]} = K_2 \quad \text{(Equation 7)}$$

$$\frac{[MOPS^-][H^+]}{[MOPS]} = K_3 \quad \text{(Equation 8)}$$

$$\frac{[NH_3][H^+]}{\left[NH_4^+\right]} = K_4 \quad \text{(Equation 9)}$$

$$[H^+][OH^-] = K_w \quad \text{(Equation 10)}$$

Please cite this article in press as: Gopalakrishnappa et al., Environmental modulators of algae-bacteria interactions at scale, Cell Systems (2024), https://doi.org/10.1016/j.cels.2024.08.002

$$2a + b + [TrisH^+] + [H^+] + \left[NH_4^+\right] = 2\left[HPO_4^{2-}\right] + \left[HPO_4^-\right] + x + [OH^-] + [MOPS^-] + d \quad \text{(Equation 11)}$$

Equations 2, 3, 4, and 5 are atom conservation. Equations 6, 7, 8, 9, and 10 are chemical equilibrium, where K_1, K_2, K_3, K_4 are equilibrium constants between weak acids ($H_2PO_4^-$, $TrisH^+$, MOPS, NH_4^+ and their conjugate bases (HPO_4^{2-}, Tris, $MOPS^-$, NH_3), and K_w is the equilibrium constant of water. Equation 11 is the charge conservation. Solving the equation gives

$$x = \frac{[H^+]}{K_1+[H^+]}a - \frac{K_1}{K_1+[H^+]}b + \frac{[H^+]}{K_2+[H^+]}c - \frac{K_3}{K_3+[H^+]}d + [H^+] - \frac{K_w}{[H^+]} - \frac{K_4}{K_4+[H^+]}e \quad \text{(Equation 12)}$$

Acetate and pyruvate have buffering effects too when used as carbon sources. When f mol of sodium pyruvate having equilibrium constant of K_5 is present, the titration curve is calculated similarly:

$$x = \frac{[H^+]}{K_1+[H^+]}a - \frac{K_1}{K_1+[H^+]}b + \frac{[H^+]}{K_2+[H^+]}c - \frac{K_3}{K_3+[H^+]}d + [H^+] - \frac{K_w}{[H^+]} - \frac{K_4}{K_4+[H^+]}e \quad \text{(Equation 13)}$$

$$+ \frac{[H^+]}{K_5+[H^+]}f \quad \text{(Equation 14)}$$

When g mol of sodium acetate having equilibrium constant of k_6 is present, the titration curve is calculated similarly:

$$x = \frac{[H^+]}{K_1+[H^+]}a - \frac{K_1}{K_1+[H^+]}b + \frac{[H^+]}{K_2+[H^+]}c - \frac{K_3}{K_3+[H^+]}d + [H^+] - \frac{K_w}{[H^+]} - \frac{K_4}{K_4+[H^+]}e \quad \text{(Equation 15)}$$

$$+ \frac{[H^+]}{K_6+[H^+]}g \quad \text{(Equation 16)}$$

Table S4 shows chemical constants for all buffering agents in the experiment. Note that the equilibrium constants depend on temperature. Because equilibrium constants in the literature are often measured at $25^\circ C$, we calculate the corrected equilibrium constant at the experimental temperatures ($30^\circ C$) using the following equation[74]:

$$pK_T = pK_\theta - \frac{1}{R \ln 10}\left[\Delta H\left(\frac{1}{\theta} - \frac{1}{T}\right) + \Delta C_p\left(\frac{\theta}{T} - 1 + \ln\frac{T}{\theta}\right)\right] \quad \text{(Equation 17)}$$

Here pK is defined as $pK = -\log_{10} K$. θ denotes the reference temperature ($25^\circ C$) and T denote the temperature of interest ($30^\circ C$). R is the ideal gas constant. ΔH is the ionization enthalpy and ΔC_p is the ionization thermal capacity at constant pressure.[74]

Computing initial pH and buffering capacity

The initial pH of an environment is obtained by computationally solving the equations 12/13/14 at $x = 0$, depending upon the carbon source. For our purpose, we define buffering capacity as the quantity of HCl that drops the pH to a point just before the pH can abruptly change with [HCl]. Hence, we compute buffering capacity as the smallest x (from equations 12/13/14) where the change in the first derivative before the inflection point on the pH curve is just greater than 30 (pH/[HCl] units). This method yields buffering capacity values that agree with our definition as shown in several examples (Figure S4). We expect that our measure of buffering capacity determines the allowed acidification in the environment before the pH drops to very low values at which the microbial growth will be negatively impacted.[47,48,72] Using these definitions of initial pH and buffering capacity, we were able to compute the initial pH and buffering capacity of all the environments formed by the merging of the droplets on kChip from the model. We note that only in the case of acetate, the buffering capacity was evaluated without taking acetate into consideration. As the pK_a of acetate is ~ 4.98, the titration curve of the environments having acetate do not have the abrupt drop in the pH with an increase in [HCl] as in the examples shown in Figure S4. However, as the buffering capacity values computed for environments without acetate correspond to low values of pH ($\sim$ <6) where the microbial growth is negatively affected, using these buffering capacity values for environments with acetate agrees with our definition of buffering capacity and hence should be valid.

Correcting the initial pH

We experimentally validated our titration model for a set of environmental conditions given in Table S2 (Figure S4). We found that the predicted initial pH was in good agreement with the experimental data in cases where [MOPS] was $\sim$10 mM (Figure S5A). And the predicted initial pH deviated from the observed initial pH in cases where [MOPS]<10 mM, the deviations being high at low concentrations of Tris and at low values of experimentally observed pH. The conditions with low observed pH were also the conditions with very low buffering capacity. We speculate that the low buffering capacity could be making the environment susceptible to pH changes (from uncharacterized chemicals in the water source or atmospheric gases) and causing poor agreement between the model and data.

Please cite this article in press as: Gopalakrishnappa et al., Environmental modulators of algae-bacteria interactions at scale, Cell Systems (2024), https://doi.org/10.1016/j.cels.2024.08.002

We corrected the deviation in the predicted initial pH using linear regressions (Figure S5B). As can be observed, the qualitative nature of the disagreement between the initial pH values predicted from the model and the initial pH values obtained from the experiments, in environments with no MOPS buffer and with MOPS at ~5 mM, differed. Hence, two separate linear regressions were set up, one to correct the data with no MOPS and another to correct the data with ~5 mM MOPS. Using these regression models, the predicted initial pH values of all the environments formed on the kChip were corrected appropriately.

Linear regression analyses

Model formulation

Linear models were set up to predict the growth of microbes Y from the environmental factors - initial pH (pH), buffering capacity (BC), phosphorus concentration ($[P]$), and carbon concentration ($[C]$). As discussed in the main text, the model was formulated as follows:

$$Y = \vec{\beta}_M \begin{bmatrix} 1 \\ [P] \\ [C] \\ pH[P] \\ pH[C] \\ BC[P] \\ BC[C] \end{bmatrix} + I\vec{\beta}_I \begin{bmatrix} 1 \\ [P] \\ [C] \\ pH[P] \\ pH[C] \\ BC[P] \\ BC[C] \end{bmatrix} + \beta_A A \quad \text{(Equation 18)}$$

The variable I is the indicator variable that is 0 for all monoculture wells and 1 for co-culture wells. A represents the area of the merged droplets in the well at 68 h, as inferred by the fluorescent dye images. The area feature is included to account for the differences in the merged droplet volumes across communities. The area feature is not included with the indicator variable I as we do not expect any difference in the contribution of area to the microbial growth in monoculture and coculture. The $\vec{\beta}_M$ and $\vec{\beta}_I$ denote the vectors of monoculture and interaction coefficients for the corresponding features, and β_A represents the coefficient of the area feature A.

$$\vec{\beta}_M = \left[\beta_{1,M}, \beta_{[P],M}, \beta_{[C],M}, \beta_{pH[P],M}, \beta_{pH[C],M}, \beta_{BC[P],M}, \beta_{BC[C],M}, \beta_{[P][C],M}\right] \quad \text{(Equation 19)}$$

$$\vec{\beta}_I = \left[\beta_{1,I}, \beta_{[P],I}, \beta_{[C],I}, \beta_{pH[P],I}, \beta_{pH[C],I}, \beta_{BC[P],I}, \beta_{BC[C],I}, \beta_{[P][C],I}\right] \quad \text{(Equation 20)}$$

For each carbon source, two such regression models were set up, one for predicting the growth of *E. coli* Y^{Ec} and another for predicting the growth of *C. reinhardtii* Y^{Cr}.

Data preprocessing

The growth data from the kChip experiments was preprocessed for the regression modelling to facilitate the interpretation of the regression results, as indicated in the main text.

Firstly, we classified the growth data into the different culture types based on the following scheme:

1. The data with $N^{Ec}_{(t=0h)} > 0.5$ and $N^{Cr}_{(t=0h)} < 0.2$ were classified as *E. coli* monocultures
2. The data with $N^{Ec}_{(t=0h)} < 0.2$ and $N^{Cr}_{(t=0h)} > 0.5$ were classified as *C. reinhardtii* monocultures
3. The data with $N^{Ec}_{(t=0h)} > 0.5$ and $N^{Cr}_{(t=0h)} > 0.5$ were classified as *E. coli* - *C. reinhardtii* cocultures

Following this, the data with merged-droplets area of the community between 850 pixels and 2000 pixels at 68 h were retained (The median merged-droplets area of the communities at 68 h were in the range of 1100-1400 pixels for the different carbon sources). The discarding of the data with merged-droplets area outside of 850 pixels and 2000 pixels at 68 h removed wells that have undergone excessive evaporation. Then again, as it is not feasible to examine these large datasets one by one to remove those with imaging artifacts, stray fluorescence signals, imperfect wells on the microfluidic chip etc, the data was again filtered to account for any extreme outliers. In the case of monoculture data, the highest and the lowest 0.05% of the growth data of the microbes considering all the monoculture wells were discarded. In the case of coculture data, wells with *C. reinhardtii* growth in the highest and the lowest 0.05% of the *C. reinhardtii* growth and with *E. coli* growth in the highest 2% and lowest 0.05% of the *E. coli* growth considering all the coculture wells were discarded. This method of discarding the data ensured that the growth of the microbes in the discarded data lay well beyond the lowest and the highest median growth of the microbes across replicate environmental conditions. Overall, the above filtering schemes led to data losses of ~4.8%, ~4.5%, ~3.4%, ~8.1%, and ~4.2% in the glycerol, glucose, galactose, pyruvate, and acetate datasets respectively.

Following the removal of outliers, the yields of each microbe (*E. coli*/*C. reinhardtii*) within its culture types (monoculture/coculture) were independently Z-score normalized. That is, for each microbe within its culture type (*E. coli* monoculture/*C. reinhardtii* monoculture/*E. coli* coculture/*C. reinhardtii* coculture), the mean and standard deviation of the growth Y were computed and all of the growth data was subtracted from the mean and then divided by the standard deviation to obtain the standardized growth values.

The values of the independent variables - initial pH (pH), buffering capacity (BC), carbon concentration ($[C]$), and area (A) were also independently transformed to range from 0 to 1 for each carbon source. Only phosphorus concentrations ($[P]$) were first log-transformed (owing to the order-of-magnitude variation in the phoshporus concentrations across environments) and then scaled to range

Please cite this article in press as: Gopalakrishnappa et al., Environmental modulators of algae-bacteria interactions at scale, Cell Systems (2024), https://doi.org/10.1016/j.cels.2024.08.002

from 0 to 1 independently for each carbon source. This scaling brought the values of the independent variables to similar ranges, avoiding the domination of a variable with the highest magnitude in training the regression model.

Implementing the regressions

A weighted least squares approach was used to solve for the coefficients in Equation 18. The weighted least squares approach optimizes the cost function to find the regression coefficients by accounting for the variability in the number of data points across environments (e.g. number of wells with the same environment and culture type). In our case, the weighted least squares approach works by weighting the squared error of the data by 1/variance in growth across its replicates. Replicates here refer to wells with the same culture type (*E. coli* monoculture/*C. reinhardtii* monoculture/*E. coli*-*C. reinhardtii* coculture) and environmental condition. Consider z environments indexed by j. In each environment, we have n_j^{mono} replicate wells having monocultures and n_j^{co} replicate wells having cocultures. Within each environment, we compute a variance across monoculture replicates $\sigma^2(Y^j_{data,m})$ where $Y^j_{data,m}$ is the growth in well m having monoculture that contains environment j, and variance across coculture replicates $\sigma^2(Y^j_{data,c})$ where $Y^j_{data,c}$ is the growth in well c having coculture that contains environment j. We then optimize the following objective function:

$$\sum_{j=1}^{z}\left(\sum_{i=1}^{n_j^{mono}}\frac{1}{\sigma^2\left(Y^j_{data,m}\right)}\left(Y^j_{data,m}-\widehat{Y}^j_{model,m}\right)^2+\sum_{i=1}^{n_j^{co}}\frac{1}{\sigma^2\left(Y^j_{data,c}\right)}\left(Y^j_{data,c}-\widehat{Y}^j_{model,c}\right)^2\right) \quad \text{(Equation 21)}$$

Using the WLS function in the statsmodels package in python, two regression models, one for predicting *E. coli* growth and another for predicting *C. reinhardtii* growth, were fitted to the standardized growth data of the respective microbes in each of the wells. The fits obtained from the regressions with the pearson coefficients and the RMSE values are shown in Figure S10. And the β coefficients obtained for the regression models are shown in Figures S11 and S12. The 95% confidence intervals and the p-values of the coefficients reported here were obtained from the summary output of the regressions in python.

Computing coculture coefficients

As discussed in the main text, the monoculture coefficient $\beta_{X,M}$ and the interaction coefficient $\beta_{X,I}$ where $X \in$ ({[*P*], [*C*], *pH*[*P*], *pH*[*C*], *BC*[*P*], *BC*[*C*], [*P*][*C*]}), respectively indicate the change in the growth in monoculture per unit change in X and the change in growth per unit change in X in coculture relative to monoculture. Hence, the coculture coefficient $\beta_{X,C}$, representing the change in growth in coculture per unit change in X, can be obtained by adding $\beta_{X,M}$ and $\beta_{X,I}$. And the 95% confidence interval of a coculture coefficient $\beta_{X,C}$ was computed using the covariance matrix of the features (obtained from regression analyses output in Python) as follows:

$$\beta_{X,C} = 1.96\left(\sqrt{var\left(\beta_{X,M}\right)+var\left(\beta_{X,I}\right)+2cov\left(\beta_{X,M},\beta_{X,I}\right)}\right) \quad \text{(Equation 22)}$$

The p-values of the coculture coefficients were obtained as outlined in Altman and Bland.[75]

Hierarchical clustering of carbon sources

Two Hierarchical clusterings were performed (using Scipy (cluster.hierarchy) with Ward's distance as the linkage metric) to find similarities between the carbon sources based on

1. similarities in the microbial growth (Figure 6C, main text)
2. similarities in the regression coefficients (Figure 6B, main text)

We began by constructing the data matrices for hierarchical clusterings. In the case of (1), carbon sources formed the columns, and environmental conditions in the different culture types for each microbe type (*E. coli* monoculture/*C. reinhardtii* monoculture/*E. coli* coculture/*C. reinhardtii* coculture) formed the rows, with matrix entries the median standardized growth *Y* of *E. coli* or *C. reinhardtii* mapping to the environmental conditions, culture types, and microbe types.

In the case of (2), carbon sources formed the columns again and features with and without the indicator variable *I* i.e ([*P*], [*C*], *pH*[*P*], *pH*[*C*], *BC*[*P*], *BC*[*C*], [*P*][*C*], *I*[*P*], *I*[*C*], *IpH*[*P*], *IpH*[*C*], *IBC*[*P*], *IBC*[*C*], *I*[*P*][*C*]) in the regression models of *E. coli* and *C. reinhardtii* growth formed the rows, with matrix entries the monoculture or interaction coefficients obtained from regressing *E. coli* growth, or monoculture or interaction coefficients obtained from regressing *C. reinhardtii* growth i.e β_M^{Ec} or β_I^{Ec} or β_M^{Cr} or β_I^{Cr}, mapping to the features and the microbe type.

The correlation matrix for hierarchical clusterings was computed accounting for the error in the data. If v_k represents the column vectors of the data matrices where $k \in (1,2,3,4,5)$ represents the five carbon sources, we compute the following quantities to arrive at the correlation coefficient between v_k and v_l:

Weighted mean of $\mathbf{v_k}$ *and* $\mathbf{v_l}$.

$$\mu_{v_k} = \frac{\sum_p \frac{1}{\sigma^2(v_{kp})} v_{kp}}{\sum_p \frac{1}{\sigma^2(v_{kp})}}, \mu_{v_l} = \frac{\sum_p \frac{1}{\sigma^2(v_{lp})} v_{lp}}{\sum_p \frac{1}{\sigma^2(v_{lp})}} \quad \text{(Equation 23)}$$

Please cite this article in press as: Gopalakrishnappa et al., Environmental modulators of algae-bacteria interactions at scale, Cell Systems (2024), https://doi.org/10.1016/j.cels.2024.08.002

where v_{kp} and v_{lp} represent the p^{th} entry in v_k and v_l respectively, and $\sigma(v_{lp})$ and $\sigma(v_{kp})$ represent the standard errors/95% confidence interval (as appropriate), in the p^{th} entry in v_k and v_l respectively

Weighted covariance between $\boldsymbol{v_k}$ *and* $\boldsymbol{v_l}$.

$$cov(v_k, v_l) = \frac{\sum_p w_p (v_{kp} - \mu_{v_k})(v_{lp} - \mu_{v_l})}{\sum_p w_p} \quad \text{(Equation 24)}$$

where

$$w_p = \frac{1}{\sigma^2(v_{kp}) + \sigma^2(v_{lp})} \quad \text{(Equation 25)}$$

Then $corr(v_k, v_l)$, the correlation between the carbon sources k and l in v is computed as:

$$corr(v_k, v_l) = \frac{cov(v_k, v_l)}{\sqrt{cov(v_k, v_k) cov(v_l, v_l)}} \quad \text{(Equation 26)}$$

The correlations between all pairs of carbon sources are computed using the same formulae.

Plate experiment assaying E. coli growth on carbon sources

The growth rate of *E. coli* measured in microtiter plates in the five carbon sources are reported in Table S5. For this experiment, the bacterial culture was grown and harvested similar to how it was done for droplet experiments. The growth was assayed in the low pH, low buffering capacity media conditions formed by combining the environments E3 and E4 and in the low pH, high buffering capacity media condition formed by combining the environments E11 and E12 (Table S2), via continuous measurement of OD590 for ~68h using the Tecan infinite F200 PRO plate reader. The growth rate was inferred by fitting a straight line to the linear portion of the natural logarithm of OD in time. The initial pH and buffering capacities of the environments, along with the growth rates and OD590 (at 68 h) of *E. coli* and the final pH (at 68 h) of the cultures (measured using VWR pH paper BDH35309.606) are reported in Table S5. The final pH was measured to be different in the two environments in the case of glucose and glycerol but similar between the respective environments in the two carbon sources - the pH drop is higher in E3+E4 environment which has lower buffering capacity than the environment E11+E12 with higher buffering capacity. On the other hand, the final pH is similar in both E3+E4 and E11+E12 in the case of galactose, pyruvate, and acetate.

Discussion on variability in algal and bacterial growth in monocultures and cocultures

To compare the variation in *E. coli* and *C. reinhardtii* growth across monocultures and cocultures, we computed the fractional error as the standard error across replicates divided by the median growth of *E. coli* and *C. reinhardtii* in monocultures and cocultures in each of the environmental conditions. We find that the median fractional error across environmental conditions is ~4.5% in the case of *E. coli* monoculture growth, ~12% in the case of *E. coli* coculture growth, ~6% in the case of *C. reinhardtii* monoculture growth, and ~4.5% in the case of *C. reinhardtii* coculture growth. Therefore, we find that the variation in *E. coli* growth in coculture is higher than in the other cases.

We hypothesized that the higher variation in *E. coli* coculture growth data compared to other cases is likely due to the higher variation in the initial number of *C. reinhardtii* cells per well in coculture we observe. In agreement with this, while the variability in the initial number of *E. coli* cells per well in monoculture and coculture, and *C. reinhardtii* cells in monoculture are similar, ~50-55%, the variability in the initial number of *C. reinhardtii* cells per well in coculture is higher, ~80% (Table S7). This difference in the variation in initial cell density across culture conditions is not surprising as the variation is expected to be higher when the median cell numbers are lower, which is the case in *C. reinhardtii* coculture. Additionally, we computed correlations between the final cell density of *E. coli* and *C. reinhardtii* in monoculture and coculture, with the initial density of *E. coli* and *C. reinhardtii*, for each culture and media condition, and compared the distribution of the correlation values between the different cases (Figure S19). We find that, on average, the final cell density of *E. coli* in monoculture and coculture positively correlates with the initial cell density of *E. coli*, as expected, the same being true in the case of *C. reinhardtii*. However, the final cell density of *E. coli* in coculture is found to be negatively correlated with the initial cell density of *C. reinhardtii*. From these observations, we conclude that the higher variation in *E. coli* growth in coculture is due to the higher variability in the initial number of *C. reinhardtii* cells and the negative correlation between the two.

Analogy between Monod's growth law and our statistical model

Monod's growth law quantitatively describes the steady-state microbial growth in monoculture as a function of nutrient concentration. The simplest form of this model is as follows:

$$\dot{N} = \frac{\mu N X}{K + X} \quad \text{(Equation 27)}$$

$$\dot{X} = -\frac{Y \mu N X}{K + X} \quad \text{(Equation 28)}$$

where μ is the growth rate, K is the affinity parameter, Y is the yield coefficient, and N and X are biomass and nutrient levels respectively, with some initial quantities of biomass and nutrients. The change in biomass in this model, at long times when nutrients are fully

Please cite this article in press as: Gopalakrishnappa et al., Environmental modulators of algae-bacteria interactions at scale, Cell Systems (2024), https://doi.org/10.1016/j.cels.2024.08.002

utilized is simply $Y * X(t = 0)$. As a result, by construction, the yield coefficient Y is simply the change in biomass per unit nutrient supplied.

In our statistical framework, when the microbial growth is affected by a single factor X (e.g nutrient concentration), our statistical model takes a simple form as described in Equation 1 of the main text. The monoculture coefficient $\beta^{Ec}_{X,M}$ which describes the change in *E. coli* growth in monoculture with *X*, can be mathematically defined as follows.

$$\beta^{Ec}_{X,M} = Y^{Ec}X \quad \text{(Equation 29)}$$

Equations 27, 28, and 29 above show the similarity between the yield coefficient *Y* in Monod's growth law and the monoculture coefficient $\beta^{*}_{X,M}$ in our statistical model.

One caveat is that the yield coefficient as calculated by Monod's law and the monoculture coefficient as calculated in our model are in exact quantitative agreement only when the factor X is limiting in the regime considered. Despite this limitation, growth as a linear function of nutrient concentration, as modeled by Monod, forms the fundamental premise for our statistical modeling as well.

Experimental validation of regression coefficients in microtiter plates

We attempted to experimentally validate a few coefficients obtained from statistical modeling, in microtiter plates. We assayed for *E. coli* and *C. reinhardtii* growth in several environmental conditions in microtiter plates to validate the monoculture coefficients of BC[C] and pH[C] of *E. coli*, and the monoculture coefficient of BC[P] of *C. reinhardtii*, in the case of glucose, in particular (Figure S11B).

*Positive monoculture coefficient of **BC**[**C**] of* E. coli. A positive monoculture coefficient of BC[C] implies that the growth of *E. coli* would be higher in an environment with high buffering capacity than in an environment with low buffering capacity, for the same carbon concentration. To test this, we assayed for growth in environments with low and high buffering capacities at a set of carbon concentrations. The plot in Figure S22A indeed shows higher growth at higher buffering capacity, with the increase in growth with $[C]$ being higher in environments with high buffering capacity, in agreement with the positive coefficient of $BC[C]$.

*Negative monoculture coefficient of **pH**[**C**] of* E. coli. A negative monoculture coefficient of pH[C] implies that the growth of *E. coli* would be higher in an environment with low pH than in an environment with high pH, for the same carbon concentration. To test this, we assayed for growth in environments with low and high pH at a set of carbon concentrations. The plot in Figure S22B indeed shows higher growth at lower pH, with the increase in growth with $[C]$ being higher in environments with lower pH, in agreement with the negative coefficient of $pH[C]$.

*Positive monoculture coefficient of **BC**[**P**] of* C. reinhardtii. A positive monoculture coefficient of BC[P] implies that the growth of *C. reinhardtii* would be higher in an environment with high buffering capacity than in an environment with low buffering capacity, for the same phosphorus concentration. To test this, we assayed for growth in environments with low and high buffering capacities at a set of phosphorus concentrations. The plot in Figure S22C indeed shows higher growth at higher buffering capacity, with the increase in growth with $[P]$ being higher in environments at high buffering capacity, in agreement with the positive coefficient of $BC[P]$. Also, note that the environmental conditions in this plot differ by both pH and buffering capacity with the conditions with high buffering capacity also having high pH and the conditions with low buffering capacity also having low pH. However, the negative monoculture coefficient of $pH[P]$, which suggests lower algal growth in an environment with higher pH, is lower in magnitude compared to the positive monoculture coefficient of $BC[P]$. Therefore, higher algal growth at a higher buffering capacity for the phosphorus concentration, as suggested by the coefficient of $BC[P]$, is observed.

Investigating the buffering ability of the phosphorus source on the regression results

As phosphate, the phosphorus source in the experiments acts as both a nutrient and a buffer, we investigated if this dual nature of phosphorus source affects our regression results. Firstly, as the experimental design ensures that the environmental phosphorus levels and buffering capacity have a poor correlation between the two (Pearson correlation ~0.1), we don't expect the dual nature of phosphate to affect the regression results. To test this directly, we truncated our full dataset to remove data where phosphate acts as a buffer i.e [P]>0.01 mM ([P]<0.01 mM in the absence of other buffers offers near zero or very little buffering capacity; Table S2). We then obtained the regression coefficients of the model considering the truncated dataset. The correlations between the original regression coefficients considering the full dataset and the new regression coefficients obtained on the truncated dataset were high ~0.52 - 0.68, in all carbon sources. We conclude from this that the phosphate serving as a phosphorus source and a buffer doesn't significantly affect our conclusions inferred from regression results.

Fluorescent intensity of the barcoding dyes is insensitive to pH

We examined the pH-dependent fluorescence characteristics of the Alexa Fluor dyes utilized for barcoding purposes. Firstly, among the three fluorescent dyes - Alexa Fluor 555 (a modified form of Cy3), Alexa Fluor 594, and Alexa Fluor 647 (a modified form of Cy5), employed in our experiments, it has been reported that the NHS ester derivatives of Cy3 and Cy5 exhibit negligible (~10%) fluorescence variation over a pH range of 6.2 to 7.4, encompassing the pH values within our experimental conditions (https://help.lumiprobe.com/p/44/fluorescence_cyanine_dyes). Furthermore, the manufacturer of these dyes, Thermo Fisher Scientific, asserts that Alexa Fluor dyes display reduced pH sensitivity compared to their parent dyes (https://www.thermofisher.com/order/catalog/product/A33080).

The efficacy of the barcode clustering algorithm strongly implies that any potential pH dependence of fluorescence, if present, does not pose a hindrance. The algorithm, which relies on distinguishing the fluorescence signals of the dyes, accurately identifies the expected number of clusters/barcodes with nearly uniform representation across all barcodes (Figure S23). The result means that any pH dependence of dye fluorescence is not sufficient to inhibit clustering.

Please cite this article in press as: Gopalakrishnappa et al., Environmental modulators of algae-bacteria interactions at scale, Cell Systems (2024), https://doi.org/10.1016/j.cels.2024.08.002

Single-cell chlorophyll concentration is insensitive to variations in media conditions

We investigated whether the chlorophyll concentration of the alga *C. reinhardtii* is influenced by cellular physiology, potentially modulated by media conditions. Algal cell density within a well was assessed by dividing the total chlorophyll intensity by the per-cell chlorophyll intensity, computed as the intensity corresponding to single algal cells identified through cell segmentation (STAR Methods). If chlorophyll concentration were influenced by physiological or media conditions, one would expect differing per-cell chlorophyll intensities across media conditions. This is not what we observe. The standard deviation in the per-cell intensities across media conditions is within ~2.5% of the median in both monoculture and coculture settings for all carbon sources, with a maximum deviation of only ~ 4% observed in coculture conditions having galactose as the carbon source. This suggests that any influence of media conditions on chlorophyll concentration is minimal. Consequently, we conclude that the algal cell abundances determined using our methodology remain comparable across media conditions and are not substantially affected by any physiological differences between the media conditions.

BSA is not a substantial nutrient source to algae and bacteria

The 0.05% w/v BSA utilized in the experiments contain considerable levels of carbon and nitrogen, ~22 mM [C] and 4.5 mM [N] (calculated based on the presence of ~580 amino acids in BSA, each with an average of 5 carbon atoms and 1 nitrogen atom). Consequently, we examined whether BSA might support the growth of *E. coli* and *C. reinhardtii* in our study. Initially, we evaluated the growth of bacteria and algae with and without BSA in M9 base media in microtiter plates, monitoring GFP and chlorophyll intensity at intervals using a plate reader. Endpoint growth measurements and abundance dynamics data indicate that BSA does not substantially contribute to biomass production (Table S8; Figure S24).

Additional evidence supporting this observation can be observed by comparing the optical density (OD) measured in plates with Taub media without BSA to the cell density computed in droplets containing BSA for *E. coli*. At the lowest carbon concentration of 2 mM, we measured an OD600 of approximately ~0.04 in plates (Figures S22A and S22B), corresponding to a cell density of approximately $0.6 * 10^8$ cells/mL (assuming OD 1 corresponds to approximately $1.5 * 10^9$ cells/mL for *E. coli*[76]), which closely aligns with the cell density computed in droplets, approximately 250 cells per well (Figure S8A, light green points in the bottom right plot comparing *E. coli* growth in monoculture and coculture), totaling around $1.2 * 10^8$ cells/mL (with each well containing 2 nL of media). Furthermore, the observed increase in *E. coli* growth in droplets containing BSA, from approximately 250 cells/mL at 2 mM [C] to approximately 1200 cells/mL at 10 mM [C] (Figure S8A, light green points representing data for 2 mM [C] on the left side of the plot vs. orange points representing data for 10 mM [C] on the right side of the plot), closely correlates with the proportional increase in carbon concentration (excluding carbon content from BSA, STAR Methods). If microbes were utilizing carbon from BSA, the fold increase in cell densities would be much lower between 2 mM [C] and 10 mM [C] as the carbon concentration increases from 24 mM [C] to 32 mM [C] (considering 22 mM of BSA in addition to 2 mM and 10 mM carbon from glucose). So if BSA was a significant carbon source, and carbon is limiting, the biomass increase would be 32/24 ~ 1.3, which is not what we observe. Given that BSA also contains nitrogen, it is unlikely that this phenomenon occurs solely due to nitrogen limitation. Therefore, we conclude that BSA does not serve as a substantial nutrient source in our study.

Gas permeabilty and compound exchange in kChip platform

Acquiring experimental data regarding the permeability of gases through the kChip platform falls beyond the purview of our study. Consequently, we undertook estimates to approximate the gas limitations within droplets. Leveraging diffusion coefficients of oxygen and carbon dioxide in PDMS within the range of $10^{-9} - 10^{-10}$ m^2/s,[77,78] and considering a microwell separation distance of 30 μm, we estimated the diffusion time between kChip wells to be on the order of several seconds ($t = d^2/D$). Hence, we performed back-of-the-envelope calculations to estimate the limitation of gases in droplets. Additionally, utilizing the solubility of oxygen in freshwater at 30°C and 1 bar, estimated at approximately 8 mg/L, we deduced the oxygen gas moles within a 1 nL droplet volume to be ~ 0.25 picomoles (globalseafood.org/advocate/dissolved-oxygen-requirements-in-aquatic-animal-respiration/). Comparing this estimated oxygen availability with carbon availability in droplets (2 - 10 picomoles) suggests that oxygen diffusion could play a substantial role in modulating microbial growth and may account for observed growth discrepancies between plates and droplets (Figure S18).

Furthermore, prior experimental investigations into compound exchange between droplets revealed that depletion of free surfactant during chip loading and droplet compartmentalization through chip sealing substantially reduced chemical exchange, indicating that nutrients supplied and waste products formed predominantly reside within the droplets.[10]

QUANTIFICATION AND STATISTICAL ANALYSIS

Estimating abundances of algae and bacteria

Computing local background GFP and chlorophyll intensities

To account for any spatial and temporal variation in the background intensities in the images, we computed the background fluorescence intensities in the GFP and chlorophyll images locally. We defined rectangular regions around the droplets/wells at each of the time points. Then the local background GFP/chlorophyll intensity for a given droplet/well was obtained as the median of the top 5% of the pixel intensities in the GFP/chlorophyll images respectively in the region bounded by the rectangle but excluding the droplet/well area containing the cells.

Detection of algae and bacteria cells

The GFP and the chlorophyll images were segmented to detect algal and bacterial cells by intensity thresholding the original images on a well-by-well basis. The GFP threshold for any given well was set to 100-pixel intensity units above the local background GFP intensity computed for that well (from above). Likewise, the chlorophyll threshold for any given well was set to 500-pixel intensity units above the

Please cite this article in press as: Gopalakrishnappa et al., Environmental modulators of algae-bacteria interactions at scale, Cell Systems (2024), https://doi.org/10.1016/j.cels.2024.08.002

local background chlorophyll intensity computed for that well. We refer to the disconnected regions of GFP/chlorophyll pixels in the segmented images of GFP/chlorophyll as GFP/chlorophyll clusters respectively. These GFP/chlorophyll clusters represent the aggregated or planktonic cells of *E. coli* or *C. reinhardtii*. Using scikit-image (regionprops), we extracted the area, total fluorescence intensity, and mean fluorescence intensity (i.e intensity per pixel) of the GFP and chlorophyll clusters, used in the further analyses below.

Estimating single-cell intensities

To estimate the single-cell intensities of *E. coli* and *C. reinhartdii*, we first estimated the typical areas of a single cell of *E. coli* and *C. reinhardtii*. The distribution of the areas of the GFP and chlorophyll clusters at the first and the last time point across the kChip were plotted (Figure S2). By visual investigation of these distributions, we inferred the typical areas of a single *E. coli* cell and a single *C. reinhardtii* cell at the first time point and the last time point to be around the peak of the distributions as marked in Figure S2. On average, *E. coli* showed a decline in the single-cell areas in all the carbon sources. On the other hand, *C. reinhardtii* showed a lower reduction in the single-cell areas and only in the case of acetate and galactose.

Using the typical areas of single cells, we were able to estimate the single-cell intensities of *E. coli* and *C. reinhardtii*. To account for any difference in the single-cell intensities between monoculture and coculture, we obtained estimates of the single-cell intensities in monoculture and coculture separately. This was done by first classifying the wells as having monoculture or coculture communities as follows -

1. If a well only has GFP clusters but no chlorophyll clusters at the first time-point, the well has an E. coli monoculture community
2. If a well has no GFP clusters but only chlorophyll clusters at the first time-point, the well has a C. reinhardtii monoculture community
3. If a well has both GFP clusters and chlorophyll clusters at the first timepoint, the well has a *E. coli - C. reinhardtii* coculture community

Then, the steps for estimating the single-cell intensities for *E. coli* and *C. reinhardtii* in monoculture and coculture involved:

Computing single-cell areas of E.coli *and* C.reinhardtii *in monoculture and coculture*

Area of a single *E. coli* cell A_{Sc}^{Ec} in monoculture/coculture was estimated as the median of the areas of GFP clusters in monocultures/cocultures across the kChip with the typical single *E. coli* cell areas estimated from above. In the same way, the area of a single *C. reinhardtii* cell A_{Sc}^{Cr} in monoculture/coculture was computed considering the chlorophyll clusters. The single-cell areas were independently computed for the first and the last time points.

Computing single-cell mean intensities of E.coli *and* C.reinhardtii *in monoculture and coculture*

Mean intensity of a single *E. coli* cell MI_{Sc}^{Ec} in monoculture/coculture was estimated as the median of the mean intensities of GFP clusters in monocultures/cocultures across the kChip with the typical single *E. coli* cell areas estimated from above. In the same way, the mean intensity of a single *C.reinhardtii* cell MI_{Sc}^{Cr} in monoculture/coculture was computed considering the chlorophyll clusters. The single-cell mean intensities were also independently computed for the first and the last time points.

Finally, the intensity of a single *E. coli*/*C. reinhardtii* cell I_{Sc}^{Ec}/I_{Sc}^{Cr} in monoculture/coculture was computed by multiplying A_{Sc}^{Ec}/A_{Sc}^{Cr} with $MI_{Sc}^{Ec}/MI_{Sc}^{Cr}$ obtained in the respective culture types.

$$I_{Sc}^{Ec-mono} = MI_{Sc}^{Ec-mono} \times A_{Sc}^{Ec-mono} \quad \text{(Equation 30)}$$

$$I_{Sc}^{Ec-co} = MI_{Sc}^{Ec-co} \times A_{Sc}^{Ec-co} \quad \text{(Equation 31)}$$

$$I_{Sc}^{Cr-mono} = MI_{Sc}^{Cr-mono} \times A_{Sc}^{Cr-mono} \quad \text{(Equation 32)}$$

$$I_{Sc}^{Cr-co} = MI_{Sc}^{Cr-co} \times A_{Sc}^{Cr-co} \quad \text{(Equation 33)}$$

The estimated values of the single-cell intensities of *E. coli* and *C. reinhardtii* at the first and the last timepoint are shown in (Figure S3). We note that the median intensity of an *E. coli* cell computed this way showed a reduction in the single-cell intensity of *E. coli* from the first timepoint to the last timepoint by more than 50% in most cases. Whereas the single-cell intensity of a *C,reinhardtii* cell was more comparable between the time points, except in the case of galactose and acetate. Additionally, *E. coli* also showed a difference in the single-cell intensity between monoculture and coculture unlike *C. reinhardtii*.

Error in single-cell intensity estimates

The standard error in the single-cell intensity estimates, δI_{Sc}, in monoculture/coculture at any timepoint is calculated as follows:

$$\delta I_{Sc} = I_{Sc} \times \sqrt{\left(\frac{\delta MI_{Sc}}{MI_{Sc}}\right)^2 + \left(\frac{\delta A_{Sc}}{A_{Sc}}\right)^2} \quad \text{(Equation 34)}$$

where δMI_{Sc} and δA_{Sc} represent the standard errors in the mean fluorescence intensity and the area of the single cells of the respective microbes at the corresponding time points and in the corresponding culture types (monoculture/coculture).

Please cite this article in press as: Gopalakrishnappa et al., Environmental modulators of algae-bacteria interactions at scale, Cell Systems (2024), https://doi.org/10.1016/j.cels.2024.08.002

Obtaining abundances of algae and bacteria

We computed the abundances of the microbes in the wells by dividing their total fluorescence intensity by the appropriate single-cell intensity estimate. For example, if the community in a well was found to be a coculture community, the abundance of *E. coli* in the well was computed by dividing the total sum of the background-subtracted fluorescence intensities of the GFP clusters in the well by the single-cell intensity of *E. coli* estimated for coculture. The mathematical expressions for calculating abundances in each of the cases are given below.

Abundance of *E. coli* N^{Ec} in a well having *E. coli* monoculture community with *n* GFP clusters:

$$I_{well}^{GFP} = \sum_{i=1}^{n} I_i^{GFP}, N^{Ec} = \frac{I_{well}^{GFP}}{I_{Sc}^{Ec-mono}} \quad \text{(Equation 35)}$$

where I_i^{GFP} represents the total GFP intensity of an i^{th} GFP cluster in the well and I_{well}^{GFP} represents the total GFP intensity of all the GFP clusters in the well.

Abundance of *C. reinhardtii* N^{Cr} in a well having *C. reinhardtii* monoculture with m chlorophyll clusters:

$$I_{well}^{Chl} = \sum_{i=1}^{m} I_i^{Chl}, N^{Cr} = \frac{I_{well}^{Chl}}{I_{Sc}^{Cr-mono}} \quad \text{(Equation 36)}$$

where I_i^{Chl} represents the total chlorophyll intensity of an i^{th} chlorophyll cluster in the well and I_{well}^{Chl} represents the total chlorophyll intensity of all the clusters in the well.

Abundance of *E. coli* N^{Ec} and abundance of *C. reinhardtii* N^{Cr} in a well having *E. coli-C. reinhardtii* coculture with *n* GFP clusters and *m* chlorophyll clusters:

$$I_{well}^{GFP} = \sum_{i=1}^{n} I_i^{GFP}, N^{Ec} = \frac{I_{well}^{GFP}}{I_{Sc}^{Ec-co}} \quad \text{(Equation 37)}$$

$$I_{well}^{Chl} = \sum_{j=1}^{m} I_i^{Chl}, N^{Cr} = \frac{I_{well}^{Chl}}{I_{Sc}^{Cr-co}} \quad \text{(38)}$$

where I_i^{GFP} and I_j^{Chl} are respectively the total GFP and total chlorophyll intensity of an i^{th} GFP and j^{th} chlorophyll cluster in the well, and I_{well}^{GFP} and I_{well}^{Chl} are respectively the total GFP and the total chlorophyll intensity of all clusters in the well.

The growth of *E. coli*/*C. reinhardtii*, represented by Y^{Ec} and Y^{Cr} respectively in any well, is then obtained by subtracting the initial abundances of the microbes in the well at t = 0 h from their final abundances in the well at t = 68 h.

$$Y^{Ec} = N_{(t=68h)}^{Ec} - N_{(t=0h)}^{Ec} \quad \text{(Equation 39)}$$

$$Y^{Cr} = N_{(t=68h)}^{Cr} - N_{(t=0h)}^{Cr} \quad \text{(Equation 40)}$$

The median and standard deviation in the abundances across environmental conditions, for each carbon source and culture condition, are reported in Table S6.